RSC Advances

ROYAL SOCIETY OF CHEMISTRY

www.rsc.org/advances

RSC Advances

Review

Received 00th January 20xx,
Accepted 00th January 20xx

DOI: 10.1039/x0xx00000x

www.rsc.org/

Advances in high-capacity Li_2MSiO_4 (M = Mn, Fe, Co, Ni...) cathode material for lithium-ion batteries

H.-N. Girish and G.-Q. Shao*

The orthosilicate Li_2MSiO_4 (M = Mn, Fe, Co, Ni…) is a competitive cathode material for the next generation high-capacity (～330 mA·h·g^{-1} with a possible 2 Li^+ extraction per formula unit) rechargeable lithium-ion batteries. It is an alternative of other polyanion compounds, because the raw materials of Fe/Mn-contained oxidate and silica are abundant, cost effective, high safety, environment friendly, and its Si-O bond is at least stable as other polyoxyanion group with excellent cycling performance. This review highlights the research progress related to the Li_2MSiO_4 cathode materials on the structures with phase transition, synthesis methods and improving techniques for electrochemical performance.

Contents:

A. Introduction
B. Polymorph Structure of Li_2MSiO_4 and Phase Transition
  B. 1. Synthesis Condition for Phase Formation and Phase Transition in Li_2MSiO_4
  B. 2. Phase Transition while Charging / Discharging in Li_2MSiO_4
C. Synthesis Methods
  C. 1. Solid-State Method
  C. 2. Sol-Gel Technique
  C. 3. Hydrothermal / Solvothermal / Supercritical Fluid Techniques
  C. 4. Microwave Method
  C. 5. Spray Pyrolysis / Combustion / Hydro-Chemical Techniques
D. First Principles of Density Functional Theory (DFT) Calculations
E. Techniques for Improving the Electrochemical Performance
  E. 1. Carbon Coating
  E. 2. Optimization of the Particle Size and Morphology
  E. 3. Cation-Substitution
F. Conclusions

A. Introduction:

Lithium-ion batteries (LIBs) can effectively store energy in the form of chemicals. So far, cathode materials have become the hotspot in LIBs. The early cathode materials such as $LiCoO_2$, $LiNiO_2$, $LiMn_2O_4$, $LiMnO_2$, *et al.* have limitations related to cost, toxicity on environment, inherent chemical and thermal stability in their applications. Extensive researches can be found, which have focused on developing suitable promising cathodes [1-6], in the field of polyanion materials such as phosphates ($LiMPO_4$, $Li_3M_2(PO_4)_3$, $LiMP_2O_7$, M = Mn, Fe, Co, Ni…, same below) [7-17], silicates (Li_2MSiO_4, Li_2VOSiO_4), [18-24], fluorophosphates (Li_2MPO_4F, Li_2VPO_4F) [25], fluorosilicates (R_2SiF_6, R = K, Na, NH_4^+…), sulfates ($LiCoOSO_4$, $LiNiOSO_4$,

State Key Laboratory of Advanced Technology for Materials Synthesis and Processing, Wuhan University of Technology, Wuhan 430070, China.

**Corresponding author. Tel./Fax: +86 27 87210216. E-mail address: gqshao@whut.edu.cn (G.-Q. Shao)*

Li_2NiSO_4) [26, 27], tavorite fluorosulphates ($LiMSO_4F$) [28] and borates ($LiMBO_3$) [29-33]. Recently lithium transition-metal (TM) orthosilicate Li_2MSiO_4 (M = Mn, Fe, Co, Ni…) has been attracting considerable attention for use as a new generation cathode. It is an alternative to phosphate or a better one because of its strong Si-O covalent bond (at least stable compared to other polyoxyanion group) resulting in high chemical stability towards electrolyte. It has a high theoretical capacity (~330 mA·h·g^{-1}) which can possibly extract more than one lithium ion per formula unit (*i.e.* 1 Li^+ / f.u.) [18, 23, 34-39].

Calculations of the electrochemical potential of lithium insertion or extraction show two processes:

$Li_2M^{2+}SiO_4 \rightarrow LiM^{3+}SiO_4 + Li^+$ (1)

$LiM^{3+}SiO_4 \rightarrow M^{4+}SiO_4 + Li^+$ (2)

Depending on TM types as shown in Fig. 1, the potential in reaction (1) (green square) varies from 3.1 V (for Fe) to 4.1 - 4.6 V (for Mn, Co, Ni), while that in reaction (2) (red circle) is in range 4.5 - 5.1 V. Extraction of the 2nd Li^+ requires applying high potential above 4.5 V which is a challenge for electrolyte.

The Li_2MnSiO_4 has more advantages than Li_2FeSiO_4 in cell safety, ease of preparation and cost effectiveness. The $Mn^{3+} \leftrightarrow Mn^{4+}$ conversion provides a higher potential than the Mn^{2+}/Mn^{3+} and Fe^{2+}/Fe^{3+} (yet to be clarified whether it had an Fe^{3+}/Fe^{4+} redox couple which might just be an electrolyte degradation [18, 38, 40, 41]). During oxidation, the short Mn-O bonds in the MnO_4 tetrahedron decrease in correlation with the increase in the Mn valance state, while the long Mn-O bonds remain unchanged [42]. In practical applications, Li_2MnSiO_4 as a cathode is limited by its low electronic conductivity of ~5 x 10^{-16} S·cm^{-1} at room temperature (RT) (and ~3 x 10^{-14} S·cm^{-1} at 60 °C), which is 5 - 6 orders of magnitude smaller than that of $LiFePO_4$ at RT. The preparation of pure Li_2MnSiO_4 even up to 800 °C are not trivial due to the possible presence of the mixed phases and impurities such as MnO, $MnSiO_3$, Li_2SiO_3, *etc.* [43-46].

The Co- or Ni-contained salts are commercially expensive and environmentally toxic for preparing Li_2CoSiO_4 and Li_2NiSiO_4. Li_2NiSiO_4, with the lowest band-gap, has not the shortcoming of Mn derivatives [18]. But delithiation potentials (> 4.6 V) of Li_2CoSiO_4 and Li_2NiSiO_4 are too high to make the present electrolyte a suitable Li^+ diffusion medium. In the same way, their kinetic properties make it difficult for preparation and poor delithiation / lithiation during charge / discharge process [18, 36, 47-49].

Otherwise, the defects like poor reversibility consisted in Li_2MSiO_4 which become a huge obstacle to the extensive applications in electric vehicles (EV) and plug-in hybrid electric vehicles (PHEV) [50-53]. Various methods have been developed to increase the electrochemical properties like controlling the particle size and morphology (like nano sheet / rod-like particles) [45, 54-57], cation-substitution (Mg^{2+}, Al^{3+}, Cr^{2+}, *etc.*) [56, 58-65] and surface-coating with conductive materials [66-80]. In surface-coating methods, proper carbon coating has been widely used [81-84], because it not only improves electronic conductivity but also reduces particle size, which are favourable for enhancing electrochemical properties.

This review will explain the polymorph structure of Li_2MSiO_4 and phase transition; summarize its research progress, synthesis methods and improving techniques for electrochemical performance.

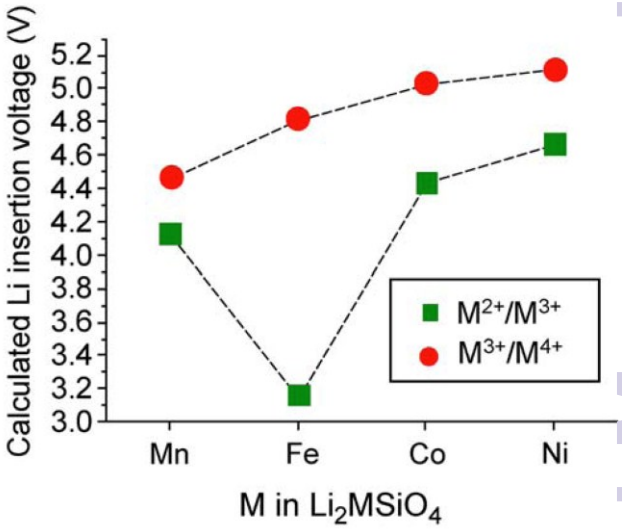

Figure 1: Variation of Li insertion voltage by M^{2+}/M^{3+} and M^{3+}/M^{4+} in Li_2MSiO_4 [18].

B. Polymorph Structure of Li_2MSiO_4 and Phase Transition:

The orthosilicate (Li_2MSiO_4) represents a family having iso-structure of tetrahedral lithiophosphate (Li_3PO_4). The crystal structure Li_2MSiO_4 consists of distorted hexagonal close-packing of oxygen ions with half tetrahedral sites occupied by Li, M and Si cations, so that face sharing between the pair of tetrahedral sites is avoided. These tetrahedral structures exhibit a rich polymorphism.

Li_3PO_4 crystallize in "α-phase formed in low temperature", "β-phase in high temperature" and "γ-phase above 1170 °C" [45, 85]. Several temperature / pressure - dependent polymorphs in Li_2MSiO_4, namely high temperature monoclinic γ_o / γ_s ($P2_1/n$) and orthorhombic γ_{II} (*Pmna, Pmnb, Cmma*, γ-Li_3PO_4), and low temperature orthorhombic β_I (*Pbn*2_1, *Pna*2_1, β-Li_3PO_4) / β_I (*Pmn*2_1, β-Li_3PO_4), can be stabilised / influenced significantly by synthesis conditions and also electrochemical cyclic behaviors [86]. These phases maybe quenched to RT and exhibit a long-term stability. Metastable monoclinic (P_n) Li_2MnSiO_4 prepared by ion-exchange from Na_2MnSiO_4 was also reported [83]. Different phase structures of Li_2MSiO_4 polymorphs are shown in Fig. 2 [38, 45, 83, 86-92] and discussed below.

(a) Orthorhombic β_{II} structure (*Pmn*2_1) and modified-inverse-β_{II} structure (*Pmn*2_1-I): All the tetrahedra end in the same direction, perpendicular to the close-packed planes, and share only corners with each other. Chains of LiO_4 are along the a-axis and parallel to chains of alternating MO_4 and SiO_4 (Fig. 2a) [45].

In the later (*e.g.* the cycled polymorph of Li_2FeSiO_4), all tetrahedra end in the same direction along the c-axis / b-axis and are linked only by corner-sharing. The SiO_4 tetrahedra are

isolated from each other, sharing corners with LiO_4 and $(Li/Fe)O_4$ tetrahedra [86, 90, 91]. These are more stable configuration in low temperature.

(b) Orthorhombic β_I structure ($Pbn2_1$, $Pna2_1$), in which all tetrahedra point in same direction with chains of alternating LiO_4 and MO_4 tetrahedra along *a*-axis, parallel to chains of alternating LiO_4 and SiO_4 tetrahedra (Fig. 2b) [38, 87-90, 92].

Quoirin *et al.* prepared an orthorhombic Li_2FeSiO_4 ($Pna2_1$, β_I) by precipitation at 100 °C in air which was optionally in the space group of *Pccn*. It might be an intermediate between the orthorhombic $Pmn2_1$ (β_{II}) and monoclinic $P2_1/n$ (γ_s) phases [87-89].

(c) Orthorhombic γ_{II} structure (*Pmna, Pmnb, Cmma*), in which the tetrahedra are arranged in groups of three with the central tetrahedron ending in the opposite direction to the outer two, with which they share edges; the group of 3 edge-sharing tetrahedra consist of the sequence Li-*M*-Li (Fig. 2c and the inset) [45].

(d) Monoclinic γ_s structure ($P2_1/n$, previously designated as $P2_1$ [93-95]), half of the tetrahedra end in reverse directions, containing pairs of LiO_4/MO_4 and LiO_4/LiO_4 edge-sharing tetrahedra (Fig. 2d and the inset) [45].

(e) Monoclinic γ_0 structure ($P2_1/n$), similar as γ_{II} structure, the group of 3 edge-sharing tetrahedra consist of the sequence Li-Li-*M* (Fig. 2e) [45].

(f) Monoclinic structure (P_n), similar as orthorhombic β_{II} structure ($Pmn2_1$), is a metastable form of Li_2MnSiO_4 and can convert to β_{II} above 370 °C. Here MnO_4 and SiO_4 tetrahedra point in the same direction parallel to their *c*-axis (Fig. 2f) [83].

Fig. 3 shows the schematic diagram of temperature / pressure - dependent polymorphs of Li_2MSiO_4 with phase transition. Table 1 shows the reported lattice parameters of Li_2MSiO_4 polymorphs (*M* = Fe, Mn, Co, Ni).

The difference among these polymorph structures are mainly depends on different arrangement of cation tetrahedra and local order (order probes such as solid-state Magic Angle Spinning Nuclear Magnetic Resonance (MAS NMR) are very useful to identify the obtained polymorphs and also the mixtures of them) [96, 97].

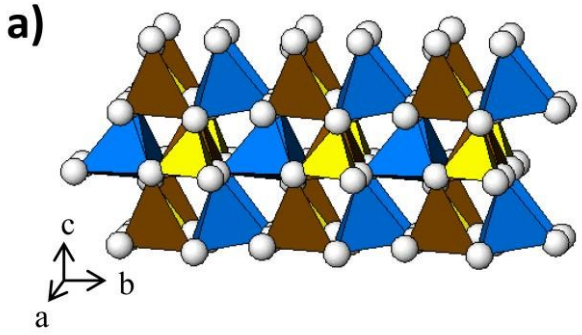

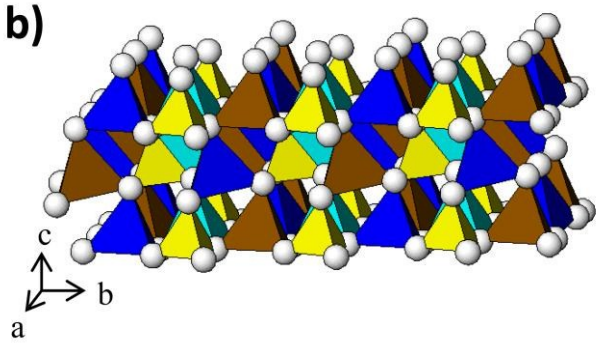

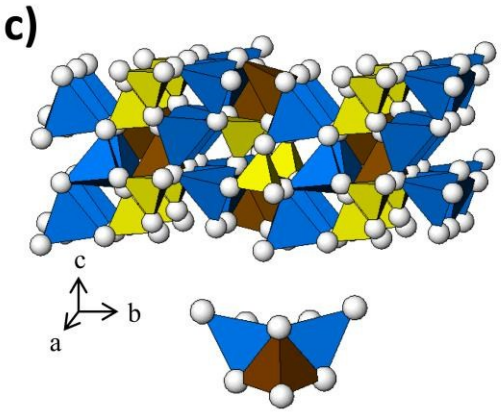

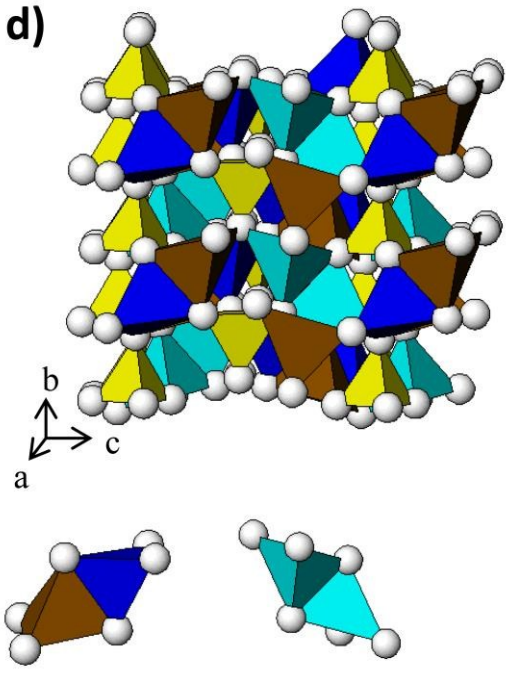

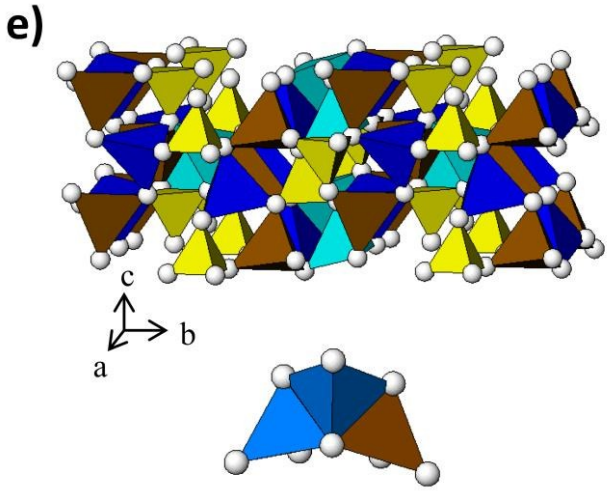

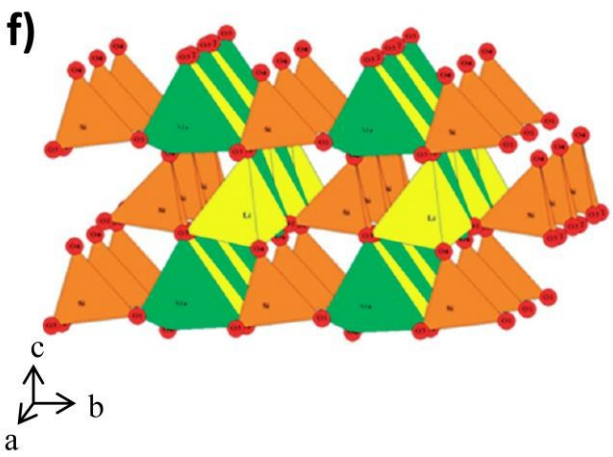

Figure 2: Structures of Li_2MSiO_4 [38, 45, 83, 86-92]: a) orthorhombic β_{II} ($Pmn2_1$); b) orthorhombic β_1 ($Pbn2_1$, $Pna2_1$); c) orthorhombic γ_{II} (*Pmna, Pmnb, Cmma*); d) monoclinic γ_s ($P2_1/$, $P2_1$); e) monoclinic γ_0 ($P2_1/n$); f) monoclinic P_n. SiO_4 (yellow); MO_4 (brown / green); LiO_4 (blue / orange); light and dark blue tetrahedra represent crystallographically distinct Li sites.

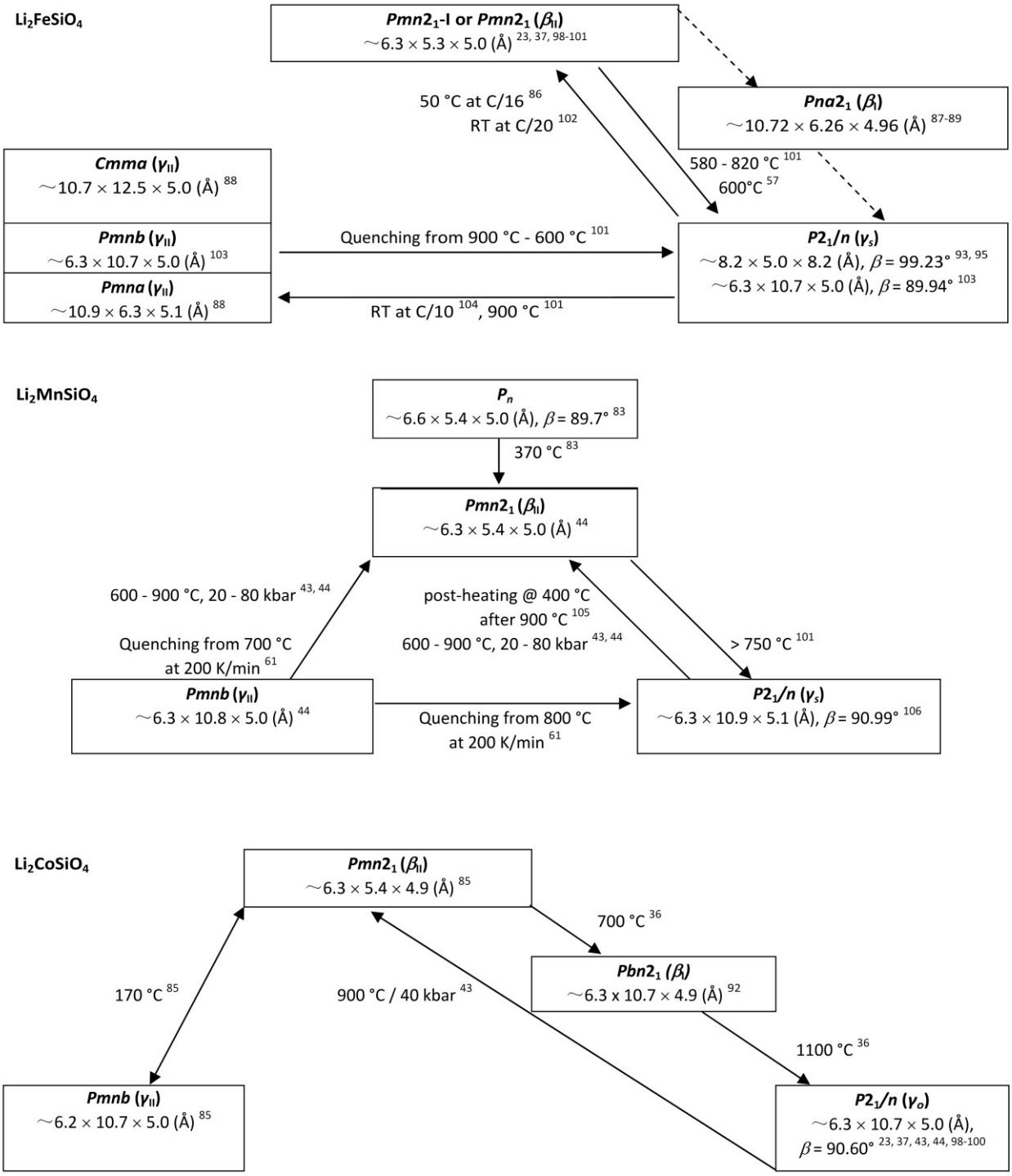

Figure 3: Schematic diagram of temperature / pressure - dependent polymorphs of Li_2MSiO_4 with phase transition.

Table 1: The reported lattice parameters of Li_2MSiO_4 polymorphs (*M* = Fe, Mn, Co, Ni).

Li_2MSiO_4	x	Space group	Crystal system	*a* / Å	*b* / Å	*c* / Å	*α* / °	*β* / °	*γ* / °	Refs.
Li_2FeSiO_4	-	$Pbn2_1$ (β_I)	orthorhombic	6.2652(1)	10.8121(1)	4.9504(1)	90	90	90	88, 89
	-	$Pna2_1$ (β_I)	orthorhombic	10.724(5)	6.260(7)	4.958(6)	90	90	90	87-89
	-	$Pmn2_1$ (β_{II})	orthorhombic	6.2709(8)	5.3382(7)	4.9651(7)	90	90	90	88, 89
	-	$Pmn2_1$ (β_{II})	orthorhombic	6.2661	5.3295	5.0148	90	90	90	23
	-	$Pmn2_1$ (β_{II})	orthorhombic	6.271(1)	5.336(1)	4.9607(9)	90	90	90	37
	-	$Pmn2_1$ (β_{II})	orthorhombic	6.3246	5.3817	4.9967	90	90	90	18
	-	$Pmn2_1$ (β_{II})	orthorhombic	6.313	5.393	4.979	90	90	90	39
	-	$Pmnb$ (γ_{II})	orthorhombic	6.2853(5)	10.6592(8)	5.0367(4)	90	90	90	103
	-	$Pnma$ (γ_{II})	orthorhombic	10.656	6.285	5.038	90	90	90	88
	-	$Cmma$ (γ_{II})	orthorhombic	10.664	12.540	5.022	90	90	90	88
	-	$P2_1/n$ (γ_s)	monoclinic	8.2253(5)	5.0220(1)	8.2381(4)	90	99.230	90	93
	-	$P2_1/n$ (γ_s)	monoclinic	6.2835(7)	10.6572(1)	5.0386(5)	90	89.941	90	103
	-	$P2_1$ (γ_s)	monoclinic	8.2278(1)	5.0204(6)	8.2295(1)	90	99.231	90	95
Li_2MnSiO_4	-	$Pmn2_1$ (β_{II})	orthorhombic	6.3109(9)	5.3800(9)	4.9662(8)	90	90	90	37
	-	$Pmn2_1$ (β_{II})	orthorhombic	6.308(3)	5.377(3)	4.988(9)	90	90	90	107
	-	$Pmn2_1$ (β_{II})	orthorhombic	6.3666	5.4329	4.0368	90	90	90	18
	-	$Pmn2_1$ (β_{II})	orthorhombic	6.308(9)	5.385(9)	4.999(6)	90	90	90	1
	-	$Pmn2_1$ (β_{II})	orthorhombic	6.3064	5.3893	4.9715	90	90	90	109
	-	$Pmn2_1$ (β_{II})	orthorhombic	6.3141	5.3702	4.9650	90	90	90	4
	-	$Pmnb$ (γ_{II})	orthorhombic	6.3126	10.7657	5.0118	90	90	90	44
	-	$P2_1/n$ (γ_s)	monoclinic	6.3368(1)	10.9146(2)	5.0730(1)	90	90.98	90	106
	-	$P2_1/n$ (γ_s)	monoclinic	6.3363(5)	10.8950(7)	5.07506(3)	90	90.99	90	44
	-	P_n (metastable)	monoclinic	6.593(5)	5.402(1)	5.090(2)	90	89.7(3)	90	83
Li_2CoSiO_4	-	$Pbn2_1$ (β_I)	orthorhombic	6.253	10.685	4.929	90	90	90	92
	-	$Pmn2_1$ (β_{II})	orthorhombic	6.2599	10.6892	4.9287	90	90	90	85
	-	$Pmn2_1$ (β_{II})	orthorhombic	6.159	5.440	4.988	90	90	90	110
	-	$Pmn2_1$ (β_{II})	orthorhombic	6.287(6)	5.353(1)	4.937(1)	90	90	90	47
	-	$Pmn2_1$ (β_{II})	orthorhombic	6.267(9)	5.370(8)	4.939(4)	90	90	90	47
	-	$Pmn2_1$ (β_{II})	orthorhombic	6.2015	5.4378	4.9909	90	90	90	18
	-	$Pmnb$ (γ_{II})	orthorhombic	6.20	10.72	5.03	90	90	90	85
	-	$P2_1/n$ (γ_o)	monoclinic	6.284	10.686	5.018	90	90.60	90	43
Li_2NiSiO_4	-	$Pmn2_1$ (β_{II})	orthorhombic	6.2938	5.3702	4.9137	90	90	90	18
	-	$Pmn2_1$ (β_{II})	orthorhombic	6.274	5.365	4.921	90	90	90	1
	-	$Pmn2_1$ (β_{II})	orthorhombic	6.290	5.299	4.856	90	90	90	112
$Li_2(Fe_{1-x}Mn_x)SiO_4$ (x = 0, 0.3, 0.5, 0.7, 1)	x = 0	$Pmn2_1$ (β_{II})	orthorhombic	6.2512	5.3425	5.0188	90	90	90	113
	x = 0.3			6.2117	5.381	4.975				
	x = 0.5			6.2581	5.3747	5.006				
	x = 0.7			6.2851	5.381	5.0012				
	x = 1			6.3099	5.394	5.0192				
$Li_2(Mn_{1-x}Fe_x)SiO_4/C$ (x = 0, 0.2, 0.5, 0.8)	x = 0	$Pmn2_1$ (β_{II})	orthorhombic	-	-	-	90	90	90	109
	x = 0.2			-	-	-				
	x = 0.5			-	-	-				
	x = 0.8			-	-	-				
$Li_2(Fe_{1-x}Mn_x)SiO_4$ (x = 0, 0.2, 0.5, 1)	x = 0	$P2_1/n$ (γ_s)	monoclinic	8.244(8)	5.004(4)	8.244(8)	90	99.25	90	102
	x = 0.2	$P2_1/n$ (γ_s)	monoclinic	8.264(7)	5.020(7)	8.264(4)	90	99.00	90	
		$Pmnb$ (γ_{II})	orthorhombic	6.591(6)	9.462(7)	4.988(1)	90	90	90	
	x = 0.5	$Pmn2_1$ (β_{II})	orthorhombic	6.284(0)	5.391(9)	5.015(1)	90	90	90	
		$P2_1/n$ (γ_s)	monoclinic	6.986(8)	8.030(9)	5.990(4)	90	95.19	90	
	x = 1	$Pmn2_1$ (β_{II})	orthorhombic	6.299(9)	5.381(5)	4.974(2)	90	90	90	
		$Pmnb$ (γ_{II})	orthorhombic	5.929(5)	10.622(0)	4.961(1)	90	90	90	
		$P2_1/n$ (γ_s)	monoclinic	6.305(7)	11.098(7)	5.114(9)	90	92.44	90	
$Li_2(Fe_{1-x}Mn_x)SiO_4/C$ (x = 0, 0.05, 0.1, 0.2, 0.3)	-	$Pmn2_1$ (β_{II})	orthorhombic	-	-	-	90	90	90	114
$Li_2(Fe_{0.5}Mn_{0.5})SiO_4$	-	$Pmnb$ (γ_{II})	orthorhombic	-	-	-	90	90	90	1
$Li_2(Fe_{0.5}Mn_{0.5})SiO_4/C$	-	$Pmn2_1$ (β_{II})	orthorhombic	-	-	-	90	90	90	106

B. 1. Synthesis Condition for Phase Formation and Phase Transition in Li_2MSiO_4:

The structures of Li_2MSiO_4 materials from different synthesis methods further affect on lithium intercalation behavior [116]. Among various polymorphs, Li_2MSiO_4 with $P2_1$ symmetry has higher electronic conductivity [48]. But both high / low temperature orthorhombic structures are more stable than the monoclinic ones [44].

Orthorhombic β_{II}-Li_2MSiO_4 ($Pmn2_1$) formed at low temperature (150 - 200 °C) *via* hydrothermal methods [100, 117-120], and at 600 - 800 °C *via* solid-state [37, 73, 81, 99, 121-128], sol-gel [41, 57, 78, 84, 108, 129-138], spray pyrolysis [139, 140], microwave [141], combustion [142] methods, *etc.* It is much stable and easy to be synthesized in all techniques. For examples, β_{II}-Li_2CoSiO_4 was obtained *via* a hydrothermal technique at 150 °C and treatment at 700 °C [143], *via* a combustion route at 950 °C [144] and *via* a supercritical technique at 350 °C / 38 MPa [145].

Orthorhombic β_I-Li_2MSiO_4 ($Pbn2_1$, Yamaguchi *et al.* nominated it as β_{II}-$Pbn2_1$ [92] previously) formed at higher temperature than β_{II}-$Pmn2_1$ and only few data's had been reported for this phase [143-145]. To the best of my knowledge, this phase is not yet reported in Li_2MnSiO_4.

Monoclinic γ_s-Li_2MSiO_4 ($P2_1/n$) formed at higher temperature than β_I- and β_{II}-phases with temperature range 650 - 900 °C *via* solid-state [43, 65, 79, 82, 105], sol-gel [56, 61, 63, 129, 146] and combustion [43, 147, 148] methods. When temperature further increased to 800 - 1000 °C, orthorhombic γ_{II}-phase (*Cmma* [87, 88], *Pnma* [149] or *Pmnb* [44, 85, 87, 88, 100, 103, 129, 150]) followed.

β-phase is more stable than γ-phase because the later has a larger volume and requires higher temperature for preparation and quenching [44].

Li_2FeSiO_4 (LFS): The Li_2FeSiO_4 crystallises in the orthorhombic β_{II} ($Pmn2_1$), orthorhombic γ_{II} (*Pmnb*) and monoclinic γ_s ($P2_1/n$) phases. The inverse-β_{II} structure ($Pmn2_1$-I, β_{II}) commonly formed at low temperature. The monoclinic and orthorhombic structures stabilized depending on the synthesis methods at different temperature and carbon-coating technique [42, 151].

Nyten *et al*. obtained a full pure orthorhombic β_{II}-Li_2FeSiO_4 ($Pmn2_1$) *via* a solid-state method [23, 99, 152, 153]. Quoirin *et al*. synthesized orthorhombic β_I-Li_2FeSiO_4 ($Pna2_1$) *via* a wet chemical method at 100 °C, and orthorhombic γ_{II}-Li_2FeSiO_4 at 800 °C (*Cmma*) / 900 °C (*Pnma*) *via* a solid-state method [87-89]. Nishimura *et al*. prepared monoclinic γ_s-Li_2FeSiO_4 at 800 °C ($P2_1/n$) [93-95]. Sirisopanaporn *et al.* obtained orthorhombic γ_{II}-Li_2FeSiO_4 (*Pmnb*) at 900 °C that differs from the monoclinic γ_s-phase by quenching from 800 °C [93, 103]. Bini *et al.* synthesized pure monoclinic γ_s-Li_2FeSiO_4 ($P2_1/n$) at 650 °C and pure orthorhombic γ_{II}-Li_2FeSiO_4 (*Pmnb*) at 900 °C *via* a sol-gel method [129].

At 580 °C, complete phase transformation (started at 400 °C) from orthorhombic ($Pmn2_1$, β_{II}) to monoclinic ($P2_1/n$, γ_s) was observed and it maintained up to 820 °C. Above 900 °C, phase transformed again into an orthorhombic one (*Pmna*, γ_{II}). This involved a statistical distribution of Li and Fe over the three (2/3 Li and 1/3 Fe) cation sites. By quenching orthorhombic phase (*Pmna*, γ_{II}) from 900 °C, the monoclinic one ($P2_1/n$, γ_s) was fully back at 600 °C and maintained down to RT [101]. Nano rods of orthorhombic Li_2FeSiO_4 ($Pmn2_1$, β_{II}) was prepared at 200 °C for 6 days and the phase transformed to monoclinic one ($P2_1/n$, γ_s) by heating at 600 °C [57].

Li_2MnSiO_4 (LMS): There are four polymorphs of Li_2MnSiO_4 that form at ambient pressure among. Two of them are orthorhombic β_{II} and γ_{II} (*i. e.*, $Pmn2_1$ and *Pmnb*). Another two are monoclinic $P2_1$ (γ_s) and P_n.

Politaev *et al*. synthesized monoclinic ($P2_1/n$) Li_2MnSiO_4 at 950 - 1050 °C *via* a solid-state method [106]. As mentioned before, the monoclinic P_n phase would transform to a stable orthorhombic phase ($Pmn2_1$) above 370 °C [83]. By rate cooling, reversible phase transition can be observed in Li_2MnSiO_4. The sample (*Pmnb*) prepared at 800 °C *via* a solid-state method transformed to a $P2_1/n$ phase when it cooled to RT at 20 K/min, but the sample prepared at 700 °C formed *Pmn*2$_1$ phase. This strongly indicated that the *Pmnb* phase transformed an orthorhombic disordered wurtzite-type structures [61].

Bini *et al.* synthesized pure orthorhombic β_{II}-Li_2MnSiO_4 ($Pmn2_1$) at 650 °C and mixed phases of orthorhombic γ_{II} (*Pmnb*) / monoclinic γ_s ($P2_1/n$) at 900 °C *via* a sol-gel method [129].

By a hydrothermal technique and heating at 700 °C, orthorhombic Li_2MnSiO_4 ($Pmn2_1$, β_{II}) was synthesized. Above 750 °C, it changed into monoclinic ($P2_1/n$, γ_s) phase by the discontinuity in the *c* lattice parameter [101]. By high pressure and high temperature process, phase transition can be observed with minimum impurities. The mixed phase of Li_2MnSiO_4 polymorphs, *i.e. Pmnb* and $P2_1/n$ (63 : 13 w/w) was prepared at 900 °C / 10 hrs by slowly heating (2 °C/min) with small impurities of MnO and Li_2SiO_3. At 60 kbar / 600 °C, mixed phase transformed to a $Pmn2_1$ phase, being stable at 80 kbar / 900 °C with new impurity of Mn_2SiO_4 [43].

The low-temperature orthorhombic forms are more stable (due to large volume) than the monoclinic one, which can only be prepared above 900 °C [44, 97]. By increasing the process pressure / temperature, pholymorphic transformation ($Pmn2_1$ → *Pmnb* → $P2_1/n$) will be taken place [44, 144].

Li_2CoSiO_4 (LCS): By varying the cooling rate, different polymorphs can form in Li_2CoSiO_4. Rapid cooling (0.5 °C/min) from above 1000 °C resulted in the formation of *Pmnb* (γ_{II}), while slow cooling (0.1 °C/min) formed $P2_1/n$ (γ_o). $Pmn2_1$ (β_{II}) formed by static heating of any other phases at 640 - 800 °C fallowed by quenching, and $Pbn2_1$ (β_I) formed by slow cooling of $Pmn2_1$ (β_{II}) [85].

Monoclinic Li_2CoSiO_4 ($P2_1/n$, γ_o) was prepared at 950 °C and could transform (at 900 °C) into orthorhombic $Pmn2_1$ (β_{II}) and $Pbn2_1$ (β_I) phases under 40 / 60 kbar, respectively. Both cell volumes are smaller than the monoclinic one [43]. Orthorhombic Li_2CoSiO_4 ($Pmn2_1$, β_{II}) was synthesized hydrothermally (150 °C / 72 hrs). It transformed to orthorhombic ($Pbn2_1$, β_I) phase when heated at 700 °C / 2 hrs and to monoclinic ($P2_1/n$, γ_o) phase at 1100 °C / 2 hrs [36]. Otherwise, considerable slow phase

transition from $\beta_{II} \leftrightarrow \gamma_{II}$ at 170 °C had been determined by DTA study [85].

Li_2NiSiO_4 (LNS): Similar to the others in the family of Li_2MSiO_4, Li_2NiSiO_4 was most frequently observed to be an orthorhombic structure (*Pmn*2_1, β_{II}). The DFT calculations predict that Li_2NiSiO_4 has very high de-intercalation voltages (4.5 V for Ni^{2+}/Ni^{3+} and 5.2 V for Ni^{3+}/Ni^{4+}). It confronted with big difficulty for delithiation / lithiation during charge / discharge process, even though Li_2NiSiO_4 phase had been successfully synthesized [18, 111, 112].

$Li_2(Mn_{1-x}Fe_x)SiO_4$ / $Li_2(Fe_{1-x}Mn_x)SiO_4$: This polymorphism reflects behaviors of the end-members. For Fe-rich compositions, there is a gradual transition from Fe-like behavior to Mn-like behavior with increasing Mn-content [98]. For Mn-rich compositions, there is a gradual transition from Mn-like behavior to Fe-like behavior with increasing Fe-content [102, 109, 113].

$Li_2(Fe_{1-x}Mn_x)SiO_4$ (x = 0, 0.2, 0.5, 1) were prepared *via* a modified sol-gel route using polyvinylpyrrolidone (PVP) as chelating agent and carbon source. Pure monoclinic phase (*P*2_1/*n*) was obtained when x = 0. Monoclinic (*P*2_1/*n*) and orthorhombic (*Pmnb*) mixed phases were obtained when x = 0.2. Major orthorhombic (*Pmn*2_1) and minor monoclinic (*P*2_1/*n*) mixed phases were obtained when x = 0.5. Major orthorhombic (*Pmn*2_1), minor orthorhombic (*Pmnb*) and minor monoclinic (*P*2_1/*n*) mixed phases were obtained when x = 1 [102]. However, $Li_2(Fe_{1-x}Mn_x)SiO_4$ (x = 0, 0.3, 0.5, 0.7, 1) *via* a citric assistant sol-gel technique could all be indexed to the orthorhombic phase (*Pmn*2_1), and their lattice parameters are similar [113]. All samples of $Li_2(Fe_{1-x}Mn_x)SiO_4$/C (x = 0, 0.05, 0.1, 0.2, 0.3) *via* a solution route exhibited an orthorhombic phase (*Pmn*2_1) with small amount of impurities like Fe_3O_4 and Li_4SiO_4 [114].

$Li_2(Mn_xFe_{1-x})SiO_4$ (x = 0, 0.2, 0.5, 0.8) were prepared *via* a combination of spray pyrolysis at 400 °C and wet ball milling followed by annealing at 600 °C in N_2 for 4 h. They exhibited a major orthorhombic phase (*Pmn*2_1) and small amount of impurities like FeO and SiO_2 found in materials with high Fe contains of 0.5 and 0.8 [109].

The thermal behavior of $Li_2(Fe_{0.5}Mn_{0.5})SiO_4$ *via* a sol-gel route, from RT to 950 °C, exhibited a major *Pmnb* phase (determined by *in situ* XRD) over the explored temperature range. Pure and stable *Pmnb* phase formed at 950 °C [115].

$Li_2(Fe_{0.5}Mn_{0.5})SiO_4$/C was prepared using precursors of Li_2FeSiO_4 and Li_2MnSiO_4 *via* a sol-gel route followed by heating at 600 °C for 10 hrs. It exhibited an orthorhombic phase (*Pmn*2_1) but the atomic ratio was not maintained [106].

B. 2. Phase Transition while Charging / Discharging in Li_2MSiO_4:

The rich polymorphism in Li_2MSiO_2 with the associated small transition energies is the main factor for the long-term cyclability. The phase transformation has structural, cyclic rate, applied current density, temperature and pressure dependence [43, 100]. The extraction / insertion of the 1st lithium out / into the host structure corresponds to the reaction $Li_2M^{2+}SiO_4 \rightarrow LiM^{3+}SiO_4 + Li^+ + e^-$ and is accompanied by the gradual changes of the local environment of Li nuclei from the initial Li^+-O-M^{2+} to Li^+-O-M^{3+} bonds and upon battery discharging. During discharge, phase transition can be observed with decrease in the crystal size upon the cycling. The residual M^{3+} could explain the difference in the observed NMR spectra between the fully discharged sate and the pristine state [102]. The variations in the arrangements of MO_4 in the form of orientation, size and distortion, the influence on the equilibrium potential were measured during the first oxidation M^{2+} into M^{3+} in all polymorphs. The stronger *M*-O bonds result in the higher splitting energy between bonding and antibonding states, which reduces the M^{2+}/M^{3+} redox potential *vs.* Li^+/Li^0 [100, 154]. An irreversible phase transformation was observed during the first charge, which accompanied a characteristic potential drop [23, 99, 104]. XRD study and theoretical calculations also suggested structural rearrangements involving the interchange of some *M* and Li sites [99]. Applied current density is important to kinetic phase transformation in the galvanostatic measurement [39, 100].

When the lithium ions were fully extracted from Li_xMSiO_4 (*M* = Mn, Fe, Co, Ni...), larger volume expansion was found in the Fe-/Co-/Ni-systems compared to the Mn-system [111].

Based on the structural characterization of the *Pmn*2_1-delithitated materials, Thomas *et al.* suggested that the voltage shift was due to a structural transformation of the host compound. Armstrong *et al.* suggested the Li_2FeSiO_4 phase transition from monoclinic (*P*2_1) polymorph to orthorhombic (*Pmn*2_1-I, inverse-β_{II}) phase at 50 °C and at C/16 (1C = 160 mA/g^{-1}). Chen *et al.* confirmed the same phase transition happened at RT and at C/20 [86, 102]. But the monoclinic phase could preserve even after cycling [155].

Nanocrystalline $Li_2(Fe_{1-x}Mn_x)SiO_4$/C (x = 0, 0.2, 0.5, 1) powders were tested electrochemically, and characterized using XRD, ^{7}Li MAS NMR spectroscopy, ^{57}Fe Mössbauer spectroscopy and *in situ* XAS to study the structural evolution. Results showed the materials exhibited partially reversible structural changes upon cycling. Amorphization and structural rearrangements from the initial *P*2_1/*n* polymorph to *Pmn*2_1 occurred during the 1st charge / discharge cycles. *Pmn*2_1-Li_2FeSiO_4 exhibited stable cycling performance over the subsequent 100 cycles due to the Fe^{2+}/Fe^{3+} process. A competitive redox reaction between the Mn and Fe species were deduced for $Li_2Fe_{0.8}Mn_{0.2}SiO_4$ and $Li_2Fe_{0.5}Mn_{0.5}SiO_4$. High conversion rate existed in the 1st charge from Fe^{2+} / Mn^{2+} to Fe^{3+} / Mn^{3+}, while the presence of a small fraction (< 7.5 mol%) of cations with higher oxidation state (Fe^{4+} / Mn^{4+}) could not be excluded [102].

C. Synthesis Methods:

Table 2 gives a summary of synthesis methods, particles size, morphology, experimental conditions and physicochemical / electrochemical properties of Li_2MSiO_4 (*M* = Fe, Mn, Co). High performance is observed in Li_2FeSiO_4 but yet to be clarified whether Fe^{3+}/Fe^{4+} couple could work [18, 38, 40, 41]. Besides Li_2FeSiO_4, the highest initial discharge of 313 $mA{\cdot}h{\cdot}g^{-1}$ (0.05 C, nearly 2 Li^+ extracted, 76.7% @ 20 cycles) attained in PEDOT-coated Li_2MnSiO_4 at 40 °C, which was prepared *via* a supercritical technique [156] and the second highest initial

discharge of 253.4 mA·h·g^{-1} (0.03 C) attained in Li_2MnSiO_4/C which was synthesized *via* a sol-gel technique [133].

C. 1. Solid-State Method:

High temperature is applied during this process. It appears to be quite simple, but cannot be used for all compounds due to several reasons like volatility of some raw materials and / or intermediate involved, since it is an open system. The key procedures in this method include repeating grinding and calcination, inert gas introducing, pelletization and so on. The purity and electrochemical behavior of cathode materials depend on the raw materials, growth parameters like temperature of calcination and exposure time [157, 158]. The common starting materials are compounds such as oxide, hydrate, silicate / sulfate / chloride, oxalate (M_mEt_n, salts of ethanedioic acid), acetate (M_mAc_n, salts of acetic acid), carbonate *et al.* which containing lithium, iron, manganese, cobalt and silicate elements. Sometimes tetraethyl orthosilicate (TEOS, $Si(OC_2H_5)_4$) and Li_2SiO_3 are also used. Carbon sources such as carbon black, sucrose, glucose, ascorbic acid, coal pitch [81], carbon nanosphere (CNS), carbon nanotubes (CNTs) [159], reduced graphene oxide (rGO) [127], graphene oxide (GO) [125], PEG-600 [125], cellulose acetate [125], adipic acid ($C_6H_{10}O_4$, *et al.*) , acetylene black or Ketjen black [73, 160] can be added to increase the electronic conductivity of cathodes. To the best of my knowledge, there were no publications related to the synthesis of Li_2CoSiO_4 and Li_2NiSO_4 *via* a solid-state method (but *via* others). In this technique, normal synthesis temperature for Li_2MSiO_4 ranges from 600 - 900 °C for 8 - 12 hrs. The initial discharge capacity ranges from 102 - 220.4 mA·h·g^{-1} (maximum 1.33 Li^+ extracted) at 0.06 - 1.0 C up to 100 cycles. The morphology of most resultants is agglomerate, while a few are spheres or tubes *etc.*, depending on raw materials and carbon sources. The particle size varies from 7 - 500 nm and substitution ions include V^{2+}, *etc.* [65, 114, 161, 162].

Among the cathode materials *via* a solid-state method, $Li_2Fe_{0.95}V_{0.05}SiO_4$/C exhibited the highest initial discharge capacity of 220.4 mA·h·g^{-1} (～1.33 Li^+ extracted LFS) at 0.1 C. After 50 cycles, it faded down to 146.6 mA·h·g^{-1} with retention of 78.7%**.** It was prepared by using $CH_3COOLi{\cdot}2H_2O$, $FeC_2O_4{\cdot}2H_2O$, TEOS, V_2O_5 and sucrose at 650 °C for 10 hrs [161]. Appropriate percentage of V-substitution (5 mol%) could possibly make for > 1 Li^+ extraction.

Nano spherical Li_2MnSiO_4/C/graphene exhibited a high initial discharge capacity of 215.3 mA·h·g^{-1} (～1.3 Li^+ extracted LMS) at 0.05 C (Fig. 4a). After 40 cycles, it faded down to 175 mA·h·g^{-1}. It was prepared by using $MnCO_3$, $LiOH{\cdot}H_2O$, nano SiO_2, polyethylene Glycol-600 (PEG-600), glucose, cellulose acetate, and graphene oxide at 700 °C for 10 hrs. Spherical SiO_2, mixed carbon sources and PEG-600 form 3D nest-like carbon network, which are favourable for improving the capability and cyclic stability [125].

There are some unsatisfied results reported in Li_2MSiO_4 (*M* = Mn, Co…) series prepared *via* a solid-state method where > 1 Li^+ extraction (*i.e.* capacity > 166 mA·h·g^{-1}) couldn't attain. Li_2MnSiO_4/C exhibited a low initial discharge capacity of 129 mA·h·g^{-1} at 0.06 C, which was prepared using Li_2SiO_3, $Mn(CH_3COO)_2{\cdot}4H_2O$ and sucrose at 800 °C for 12 hrs [128]. Another example is Li_2MnSiO_4 prepared from $LiCH_3COO{\cdot}2H_2O$, $Mn(CH_3COO)_2{\cdot}4H_2O$, SiO_2 and glucose at 700 °C for 10 hrs. It exhibited a low initial discharge capacity of 152 mA·h·g^{-1} [163]. The poor performance could be ascribed to impurities in samples, unsuitability of carbon source and non-excellent process (not effectively hamper the crystal structure destruction).

C. 2. Sol-Gel Technique:

It involves initial hydrolysis of homogeneous solution of one or more selected alkoxides (salts of adipic acid such as $C_6H_5FeO_7$ and $SiC_8H_{20}O_4$, *etc.*) and followed by condensation. Chelating agents / complexation such as citric acid [41, 61], sucrose [82, 147], polyethylene-poly (ethylene glycol) [153], polyvinylalcohol (PVA) [148, 164], tartaric acid [80] and ascorbic acid [165] are generally used in sol-gel technique. Synthesis temperature usually ranges 600 - 800 °C with dwell time of 5 - 15 hrs. The morphology of Li_2MSiO_4 *via* a sol-gel technique can be spherical [137, 164], mesoporous [136, 166], agglomerate [61, 63, 167], honey comb [168] *etc.*, depending on the use of chelating agents.

Most of the mesoporus structures of Li_2MSiO_4 prepared *via* a sol-gel method exhibited better discharge capacities than the other structures. Hydrochloric acids and propylene oxides used for enhancing hydrolysis of TEOS could improve capacity retention than the other chelating agents and catalysts [137, 138]. Nano particles ranging 10 - 200 nm could attain by this technique with elements substitution like V^{2+} [63], Mg^{2+} [61], Na^+ [167], Cu^{2+} [169], P^{5+} [170], Zn^{2+} [169] and Ni^{2+} [169] *etc.*.

Li_2MnSiO_4/C composite exhibited an initial discharge capacity of 240 mA·h·g^{-1} (～1.44 Li^+ extracted LMS) at 0.02 C (45.4% retention) and 125 mA·h·g^{-1} at 0.4 C (52% retention) as shown in Fig. 4b. Discharge capacity decreased with rate capacity, while retention increased. It was prepared by using $LiCH_3COO{\cdot}2H_2O$, pre-synthesized Mn_3O_4 and TEOS (2.040 : 0.763 : 2.083 wt.%) prime materials, adding acetic acid (catalyst) and sucrose (carbon source) at 700 °C for 10 hrs. Replacing solvable metal source by Mn-oxide improved cycle performance due to more compact carbon-coating and more effective restraining the side reaction between the cathode and electrolyte [130].

Li_2MnSiO_4/C nano composite exhibited a discharge capacity of 253.4 mA·h·g^{-1} (～1.53 Li^+ extracted LMS) at 0.03 C and 149.9 mA·h·g^{-1} at 1 C (56.4% retention). It was prepared by using $LiCH_3COO{\cdot}2H_2O$ (0.02 mol), $Mn(CH_3COO)_2{\cdot}4H_2O$ (0.01 mol), TEOS (0.02 : 0.01 : 0.01, mol%), water-acetic acid solution (1 : 2, wt.%) and glucose at 650 °C for 6 hrs [133]. The capacity fade may be associated with the amorphous tendency causing volumetric effect [107, 133, 171].

$Li_2(Mn_{0.94}Cr_{0.06})SiO_4$/C nanofibers exhibited a discharge capacity of 295 mA·h·g^{-1} (～1.77 Li^+ extracted LMS) at the first cycle and reached the highest capacity of 314 mA·h·g^{-1} (～1.88 Li^+ extracted LMS) at the 5th cycles. After 20 cycles, the discharge capacity was maintained at 273 mA·h·g^{-1} (～1.63 Li^+ extracted LMS). It was prepared by using N,N-Dimethylformamide (DMF), $Mn(CH_3COO)_2{\cdot}4H_2O$, $LiCH_3COO{\cdot}2H_2O$ and TEOS at 700 °C for 12 hrs. Appropriate Cr-substitution improved it's cycling behavior due to large unit

cell volume. The carbon nanofiber matrix contributed the faster electron and ion transportation, leading to good reversibility of cathode materials [64]. There are also some unfulfilled results reported in Li_2MSiO_4 (*M* = Mn, Co…) series prepared *via* a sol-gel method where > 1 Li^+ extraction (*i.e.* capacity > 166 mA·h·g^{-1}) couldn't attain. Li_2MnSiO_4 exhibited a low initial discharge capacity of 113 mA·h·g^{-1} at first cycle. It was prepared by using $LiCH_3COO{\cdot}2H_2O$, $Mn(CH_3COO)_2{\cdot}4H_2O$, TEOS and adipic acid at 700 °C [138]. Li_2CoSiO_4 exhibited only an initial discharge capacity of 32 m·h·g^{-1} at 0.02 C in the 1st cycle and it decreased after 10 cycles. It was prepared by using $LiNO_3$, $Co(NO_3)_2{\cdot}6H_2O$, silica particles and poly acrylic acid (PAA, used as a chelating agent) at 800 °C. The low capacity could be ascribed to poor electronic conductivity, insufficient ball milling and unsuitable electrolyte [164].

C. 3. Hydrothermal / Solvothermal / Supercritical Fluid Techniques:

These techniques are simple, clean, of good cost performance and less energy consumption, being suitable to prepare in close system high quality polycrystallines, *i.e.* large surface area materials with desired morphology under relatively lower temperature / pressure than those *via* a solid-state or a sol-gel techniques. The precursor concentration affects the particles' morphology and size [103, 172, 173]. Nano particles are more active materials in favour of electrochemical properties due to improved electrical conductance of the electrode, shorter diffusion paths for lithium ions within a particle and increased contact area with electrolyte [162, 174]. Normally, hydrothermal / solvothermal processes are conducted in solvent at 150 - 200 °C for 24 - 96 hrs. For complete crystallization as well as for carbon coating, products need further annealing at 600 - 700 °C for 2 - 10 hrs. The supercritical fluid technique are usually running at 300 - 400 °C / 30 - 40 MPa with very short duration of 5 - 10 min. Different morphology are observed in these techniques like flower [116, 175], spherical [118, 145, 173, 176, 177], hallow sphere [178], hierarchical [120, 179], hot-dog [180], rod [175, 177] *etc.*, depending on process conditions. The particles size varies from 5 - 400 nm. Chelating agents like citric acid ethylene glycol *etc.*, were used in hydrothermal method [37, 117, 118, 120, 176]. And some organic materials like cetrimonium bromide, ascorbic acid, urea *etc.*, were used in solvothermal method [97].

By a hydrothermal method, Mali *et al*. reported firstly three polymorphs of Li_2MnSiO_4 and their NMR spectroscopy [97]. The flower-like Li_2MnSiO_4 exhibited an initial discharge capacity of 226 mA·h·g^{-1} (～1.36 extracted LMS) at 0.05 C. After 10 cycles, the capacity was stabled at ～130 mA·h·g^{-1}. It was prepared using $LiOH{\cdot}2H_2O$, $Mn(CH_3COO)_2{\cdot}4H_2O$ and TEOS at 700 °C for 10 hrs. The flower-like particles could translate into good electrochemical properties due to their large surface area, unique morphology and high interconnections with each other [116].

By a solvothermal technique, Ni-modified Li_2MnSiO_4 (LMS@Ni/C) exhibited an initial discharge capacity of 274.5 mA·h·g^{-1} (～1.67 Li^+ extracted LMS) at 0.05 C. After 20 cycles, it faded down to 119.8 mA·h·g^{-1}. It was prepared using $C_2H_3O_2Li{\cdot}2H_2O$, $NiC_4H_6O_4{\cdot}4H_2O$, TEOS, $MnC_4H_6O_4{\cdot}4H_2O$, cetrimonium bromide (2.2 : 0.05 : 1.0 : 0.95 : 0.1, mol%) and starch at 700 °C for 10 hrs. The Ni improved ion diffusion coefficient and electronic conductivity [97].

By a supercritical technique, Li_2MnSiO_4 exhibited a very high discharge capacity of 313 mA·h·g^{-1} at 40 °C and 0.05C (～1.9 Li^+ extracted LMS) as shown in Fig. 4c. After 20 cycles, it faded down to 240 mA·h·g^{-1}. It was prepared by using $LiOH{\cdot}2H_2O$, $MnCl_2{\cdot}2H_2O$, TEOS and ascorbic acid (1 : 4 : 1 : 0.1, mol%) at 300 °C / 38 MPa for 5 min [156]. Nano Li_2MSiO_4 (*M* = Fe, Mn, Co) materials were prepared at 300 - 380 °C / 38 MPa for 5 - 30 min. They performed high discharge capacity in the 1st cycle at different rate but failed to maintain the stability [145, 156, 177]. Li_2CoSiO_4 exhibited the discharge capacity of 107 mA·h·g^{-1} (～1.51 Li^+ extracted LCS) at 0.01 C. After 3 cycles, it faded down to 80 mA·h·g^{-1}. It was prepared by using $LiOH{\cdot}2H_2O$, $CoCl_2{\cdot}6H_2O$, TEOS (4 : 1 : 1, mol%) and oleylamine at 300 - 350 °C / 30 MPa for 10 - 30 min [145].

There are a few results reported in Li_2MSiO_4 (*M* = Mn, Co, Ni…) series prepared *via* hydrothermal / solvothermal methods where > 1 Li^+ extraction (*i.e.* capacity > 166 mA·h·g^{-1}) couldn't attain. $Li_2Mn_{0.8}Ni_2SiO_4$ *via* a solvothermal technique exhibited a low discharge capacity of 100 mA·h·g^{-1} (～0.7 Li^+ extracted LMS) at 0.2 C. It was prepared by using $LiOH{\cdot}2H_2O$, $NiCl_2{\cdot}6H_2O$, $MnCl_2{\cdot}4H_2O$, SiO_2 (0.386 : 0.2 : 0.8 : 0.138, wt.%) and sucrose at 700 °C for 10 hrs. Ni-substitution maintained the structure and improved the charge capacity, but had no help to the discharge capacity [181].

C. 4. Microwave Method:

The target materials directly absorb the electromagnetic / microwave energy (self-heating) within short period of time, which is lower than in the other synthesis methods [182]. It is very fast, facile and high efficient. Nano agglomerates or spheres could be prepared at 600 - 700 °C for 6 - 20 hrs. Cathodes with high ionic conduction was obtained above RT (60 °C) [171 183, 184]. By this technique, it's difficult to extract more than 1 Li^+ from Li_2FeSiO_4 (RT) but succeeded from Li_2MnSiO_4.

By a microwave-assisted hydrothermal technique, Li_2MnSiO_4/C exhibited an initial discharge capacity of 210 mA·h·g^{-1} (～1.27 Li^+ extracted LMS) at RT and 250 mA·h·g^{-1} (～1.5 Li^+ extracted LMS) at 55 °C for 0.2 C (Fig. 4d). After 20 cycles, it drastically faded 50 % (105 mA·h·g^{-1}) at RT and 15 % (240 mA·h·g^{-1}) at 55 °C. It was prepared by using $LiOH{\cdot}2H_2O$, $Mn(CH_3COO)_2{\cdot}4H_2O$, TEOS and sucrose at 650 °C for 6 hrs [171].

Li_2MnSiO_4 *via* a microwave-assisted solvothermal synthesis exhibited an initial discharge capacity of 260 mA·h·g^{-1} at 50 °C (～1.57 Li^+ extracted LMS) and 130 mA·h·g^{-1} at RT at 0.1 C. After 4 cycles, it drastically decreased. It was prepared by using $LiOH{\cdot}2H_2O$, $Mn(CH_3COO)_2{\cdot}4H_2O$, TEOS and urea at 700 ° for 5 hrs [185].

C. 5. Spray Pyrolysis / Combustion / Hydro-Chemical Techniques:

The synthesis temperature / time vary from 600 - 800 °C for 4 - 12 hrs to form agglomerate / porous / spherical morphology, depending on conditions and carbon sources.

Spray pyrolysis method is to prepare powders with an uniform chemical composition and a narrow particle size distribution from the nanometre to the micrometer order, easily used for large-scale applications [186]. Li_2MnSiO_4 C

exhibited an initial discharge capacity of 184 mA·h·g^{-1} (～1.1 Li^{+} extracted LMS) at RT and 0.05 C. After 20 cycles, it faded down to 110.4 mA·h·g^{-1} (～60%). Moreover, it exhibited an initial discharge capacity of 225 mA·h·g^{-1} (～1.36 Li^{+} extracted LMS) at 60 °C and 0.05 C. But it faded drastically at the end of the 20th cycle [139].

Li_2MSiO_4 (*M* = Fe, Mn) were prepared *via* a combustion method, using $LiNO_3$, $Mn(CH_3COO)_2{\cdot}4H_2O$, TEOS, citric acid and 20 wt.% of acetylene black at 700 °C for 10 hrs [142]. Li_2MnSiO_4/C exhibited an initial discharge capacity of 161 mA·h·g^{-1} (～0.96 Li^{+} extracted LMS) at 0.06 C.

By a hydro-chemical technique, Li_2FeSiO_4/C/CNS with double carbon-coating (glucose-derived carbon and carbon nanosphere) exhibited an initial discharge capacity of 164.7 mA·h·g^{-1} (～1.0 Li^{+} extracted LFS) at 0.1 C. After 60 cycles, 98.4% capacity remained. It was prepared by using $CH_3COOLi{\cdot}2H_2O$, $Fe(CH_3COO)_2{\cdot}4H_2O$, TEOS, glucose and CNS at 700 °C for 12 hrs. Double carbon-coating increased the electron transport among the particles [187].

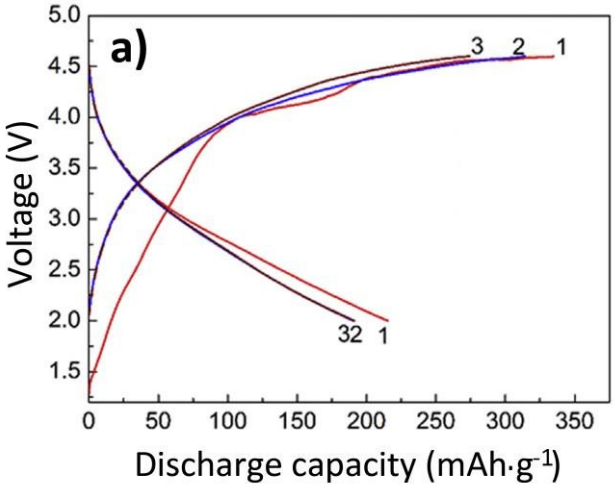

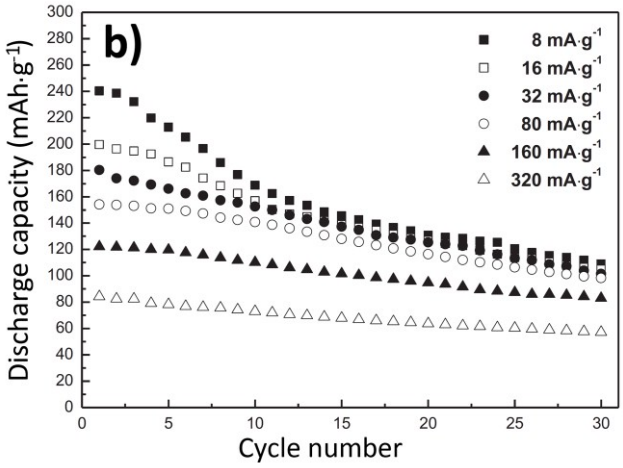

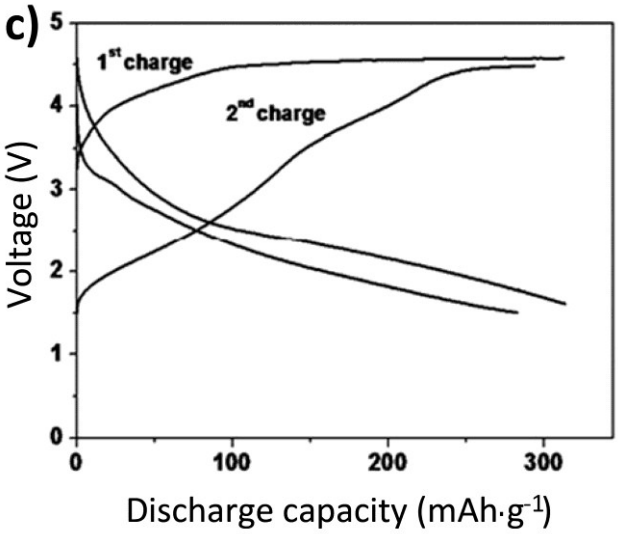

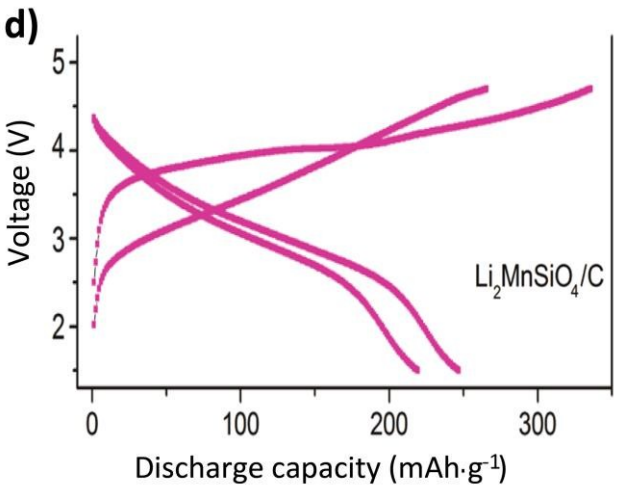

Figure 4: a) Charge / discharge profile of Li_2MnSiO_4/C/graphine (0.05 C) *via* a solid-state method [125]; b) Cyclic performance of Li_2MnSiO_4/C *via* a sol-gel technique at different current density [130]; c) Charge / discharge capacity of PEDOT/Li_2MnSiO_4 *via* a supercritical technique at 0.05 C and at 40 °C [156]; d) Charge / discharge profile of Li_2MnSiO_4/C *via* a microwave method at C/20 and 55 °C [171].

Table 2: Synthesis methods, conditions and physicochemical / electrochemical properties of Li_2MSiO_4 (M = Fe, Mn, Co)

Methods	Temp. / Time / Pressure (°C / hrs / MPa)	Morphology	Size (nm)	Specific capacity ($mA{\cdot}h{\cdot}g^{-1}$) / Current density	Retention (%) / Cycles	Refs.
Solid-state	650 / 10 / -	agglomerate (Li_2FeSiO_4/C)	-	144.8 / 0.1	94.27 / 13	188
	800 / 12 / -	agglomerate (Li_2MnSiO_4/C)	30 - 80	129 / 0.06	- / 10	128
	650 / 8 / -	agglomerate ($LiFe_{0.9}Mn_{0.1}SiO_4$/C)	-	158.1 / 0.03	94.3 / 30	114
	900 / 6 / -	agglomerate (Li_2FeSiO_4/C/rGO)	28.5	191.6 / 0.1	91.3 / 60	127
	700 / 10 / -	agglomerate ($Li_{1.95}FeSiO_4$/C/CNTs)	30 - 70	148 / 0.2	99.2 / 100	159
	700 / 8 / -	spherical (Li_2MnSiO_4/C/graphene)	50	215.3 / 0.05	81.3 / 40	125
	650 / 10/ -	agglomerate ($LiFe_{0.97}Co_{0.03}SiO_4$/C)	100 - 500	199 / 3.0	71.6 / 100	65
	700 / 15 / -	rounded (Li_2FeSiO_4/C)	200	102 / -	91.8 / 10	126
	700 / 10 / -	agglomerate ($Li_{1.95}FeSiO_4$/C)	100	142 / 1.0 / 100	95.1 / 100	122
	650 / 10 / -	agglomerate ($LiFe_{0.95}V_{0.05}SiO_4$/C)	7 - 10	220.4 / 0.1	78.7 / 50	161
	700 / 10 / -	agglomerate (Li_2MnSiO_4/C)	13.4 - 23.3	201.8 / -	73.5 / 15	163
Sol-gel	800 / - / -	spherical (Li_2CoSiO_4)	460	32 / 0.02	- / 2	164
	700 / 5 / -	spherical (Li_2MnSiO_4)	25 - 30	161 / 0.05	77.6 / 50	137
	700 / 10 / -	irregular (Li_2MnSiO_4/C)	20 - 30	240 / 0.02	45.4 / 30	130
	700 / - / -	spherical (Li_2MnSiO_4)	25 - 30	113 / -	- / 15	138
	650 / 10 / -	mesopores (Li_2FeSiO_4/C)	20 - 30	163 / 0.06	96 / 200	166
	680 / 10 / -	mesopores (Li_2MnSiO_4/C)	10 - 20	164.2 / 0.06	80 / 60	136
	650 / 10 / -	agglomerate ($Li_{1.9}Na_{0.1}MnSiO_4$/C)	30	175 / 0.01	45 / 40	167
	650 / 10 / -	agglomerate $LiFeSi_{0.9}V_{0.1}O_4$/C)	100 - 200	159 / 0.06	90 / 30	63
	700 / 12 / -	agglomerate ($LiFe_{0.97}Mg_{0.03}SiO_4$)	100	153.2 / 0.06	98.6 / 50	61
	700 / 10 / -	agglomerate ($LiMn_{0.8}Fe_{0.2}SiO_4$/C)	15 - 30	224 / 0.05	63.8 / 50	189
	700 / 10 / -	honeycomb ($Li_{1.8}MnSiO_4$)	6 - 8	147.1 / 0.03	83.3 / 25	168
	600 / 10 / -	aggregated (Li_2FeSiO_4/C-NHT)	20 - 30	195.5 / 0.1	- / 50	190
	700 / 10 / -	agglomerate ($Li_{0.5}Mn_{0.5}SiO_4$/C)	220	230.1 / 0.1	70.4 / 20	191
	700 / 12 / -	core-shell ($Li_{2.05}Mn_{0.95}P_{0.05}Si_{0.95}O_4$)	30 - 60	170 / 0.06	- / 60	170
	700 / 12 / -	agglomerate ($LiFe_{0.97}Zn_{0.03}SiO_4$)	100	128 / 0.1	97.5 / 55	169
	650 / 10 / -	mesopores (Li_2FeSiO_4@CMK-3)	50	160 / 0.1	- / 80	192
	600 / 10 / -	agglomerate (Li_2FeSiO_4/C)	15	187 / 0.1	- / 50	193
	700 / 10 / -	agglomerate ($Li_{2.05}Fe_{0.95}P_{0.05}Si_{0.95}O_4$/C)	50 - 100	213 / 0.3	- / 50	194
	650 / 6 / -	spherical (Li_2MnSiO_4/C)	20 - 50	253.4 / 0.03	77 / 20	133
	600 / 10 / -	nano wire (Li_2MnSiO_4/C/V_2O_5)	30	277.0 / 0.1	- / 50	195
	700 / 12 / -	nano fibers ($LMn_{0.94}Cr_{0.06}SiO_4$/C)	70 - 150	295 / -	65.8 / 50	64
	650 / 10 / -	agglomerate ($LiMn_{0.09}Ti_{0.01}SiO_4$)	~50	211 / 0.01	- / 50	196
Hydrothermal / Solvothermal / Supercritical	150 / 92 / -	flower (Li_2FeSiO_4)	20 - 50	130 / 0.1	- / 30	117
	700 / - / -	flower (Li_2MnSiO_4/C)	-	100 / 0.05	- / 40	162
	550 / 5 / -	spherical (Li_2MnSiO_4)	644	177 / -	32 / 20	173
	650 / 10 / -	hollow spheres (Li_2FeSiO_4)	0.5 - 2 μm	152 / 0.05	- / 100	178
	600 / 6 / -	hot-dog (Li_2FeSiO_4)	200	150 / -	- / 50	180
	900 / 4 / -	hollow spheres (Li_2CoSiO_4/C)	300 - 400	33 / -	- / 50	49
	600 / 5 / -	agglomerate (Al-$LiFe_{0.5}Mn_{0.5}SiO_4$/C)	20 - 100	216 / 0.01	- / 20	62
	200 / 72 / -	spherical (Li_2FeSiO_4/C)	~20	136 / 0.2	96.1 / 100	118
	700 / 10 / -	flower (Li_2MnSiO_4)	20	226 / 0.5	- / 10	116
	650 / 10 / -	shuttle-like (Li_2MnSiO_4/C)	0.4 - 0.5 μm	206 / 0.05	- / 50	132
	180 / 192 / -	hierarchical shuttle (Li_2FeSiO_4)	31.8	159.4 / 0.01	97.5 / 20	120
	600 / 2 / -	nano-rod (Li_2FeSiO_4/C)	80 - 100	155 / 0.06	- / 50	175
	650 / 10 / -	spherical (Li_2FeSiO_4/C)	18.3	211.3 / 0.1	97.7 / 1000	176,
	700 / 10 / -	plate ($LiMn_{0.8}Ni_{0.2}SiO_4$)	100	100 / 0.2	- / 10	181
	600 / 10 / -	3D porous hierarchical (Li_2FeSiO_4/C)	~60	170 / 0.1	- / 20	179
	600 / 06 / -	Nano-rod (Li_2FeSiO_4/graphene)	10 - 25	306.4 / 0.3	95 / 240	57
	700 / 10 / -	agglomerate (Li_2MnSiO_4@Ni)/C	20 - 50	274.5 / 0.05	- / 20	97
	700 / 5 / -	spherical (Li_2MnSiO_4)	15 - 500	260 / 0.1	- / 5	185
	380 / 30 min / 38	rod (Li_2FeSiO_4)	20 - 80	177 / 0.01	- / 25	177

	350 / 30 min / 38	spherical (Li_2CoSiO_4)	20 - 15	107 / 0.1	- / 4	[145]
	300 / 5 min / 38	spherical (Li_2MnSiO_4)	5 - 20	313 / 0.05	76.7 / 20	[156]
	400 / 4 min / 38	hierarchical nano (Li_2MnSiO_4)	4 - 5	291 / 0.05	- / 50	[197]
						[198]
Microwave	650 / 6 / -	nano sphere (Li_2FeSiO_4/C)	~20	148 / 0.05	- / 20	[171]
	650 / 6 / -	agglomerate (Li_2MnSiO_4/C)	~20	210 / 0.05	- / 20	[171]
	700 / 20 / -	agglomerate (Li_2FeSiO_4)	-	116.2 / 0.05	- / 10	[183]
	700 / 20 / -	agglomerate (Li_2FeSiO_4)	-	116.9 / 0.05	- / 10	[184]
Spray pyrolysis / Combustion / Hydro-chemical	800 / 4 / -	agglomerate (Li_2MnSiO_4/C)	~50	184 / 0.05	- / 20	[139]
	700 / 10 / -	spherical (Li_2FeSiO_4/C)	1 - 5 μm	123 / 1.0	98.4 / 300	[199]
	600 / 4 / -	spherical (Li_2FeSiO_4/C)	65	154 / 0.05	- / 70	[200]
	600 / 4 / -	agglomerate ($LiFe_{0.5}Mn_{0.5}SiO_4$/C)	65	149 / 1.0	- / 50	[109]
	700 / 12 / -	agglomerate (Li_2FeSiO_4/C/C-nanosphere)	~200	164.7 / 0.1	98.4 / 60	[187]
	650 / 10 / -	porous (Li_2FeSiO_4/C)	28	135 / 0.06	- / -	[148]
	800 / 10 / -	agglomerate (Li_2FeSiO_4/C)	29	130 / 0.06	- / 50	[147]
	700 / 10 / -	agglomerate (Li_2MnSiO_4/C)	50	164 / 0.01	- / 20	[142]

D. First Principles of Density Functional Theory (DFT) Calculations:

The first principles density functional theory (DFT) is an approach to the quantum mechanical many-body problem, where the system of interacting electrons is mapped onto an effective non-interacting system with the same total density. The total energies of all the compounds were usually calculated using the Projector Augmented Wave (PAW) formalism as implemented in the Vienna *Ab initio* Simulation Package (VASP), or the full-potential linear augmented plane wave (FP-LAPW) method, with the exchange and correlation energies approximated in Perdew-Burke-Ernzerh generalized gradient approximation (PBE-GGA), local spin density approximation (LSDA), generalized gradient and local density approximations plus an on-site Coulomb self-interaction correction potential / ultrasoft pseudopotential (GGA + U^{SIC} and LDA + U^{SIC}, respectively). Two versions of spin-polarized (ferromagnetic / anti-ferromagnetic, *i.e.* FM / AFM) calculations were employed [4420196, 202-205].

Through DFT calculations from a specific structure, properties of Li_2MSiO_4 (*M* = Mn, Fe, Co, Ni…) can be accurately predicted and reaction mechanisms can be fully described. The applications of DFT calculations include crystal structure modeling and stability investigations of delithiated and lithiated phases, average lithium intercalation voltage, prediction of charge distributions and band structures, and kinetic studies of lithium ion diffusion processes (Li^+ vacancy migration barriers [86, 206]), which can provide atomic understanding of the capacity, reaction mechanism, rate capacity, and cycling ability. The results obtained from DFT are valuable to establish the relationship between the structure and the electrochemical properties, promoting the design of new electrode materials [201].

The total energy *vs.* volume of Li_2MnSiO_4 polymorphs (orthorhombic β_{II}-*Pmn*2$_1$ / γ_{II}-*Pmnb* and monoclinic γ_s-*P*2$_1$/*n*) and their electrochemical properties as electrode for LIBs were investigated by Arroyo-de Dompablo *et al.* [44], combining experimental and computational methods. Calculation results show that the crystal structure affects little to the average Li^+ intercalation voltage (4.18 / 4.19 / 4.08 V for *Pmnb* / *Pmn*2$_1$ / *P*2$_1$/*n*, respectively). The *Pmnb* form is 2.4 / 65 meV/f.u. more stable than the *Pmn*2$_1$ / *P*2$_1$/*n* forms, respectively (Fig. 5, GGA + U results). But one can not deny that other varieties of β- and/or γ-Li_3PO_4 could be energetically accessible. In fact, a β-Li_3PO_4 (β_I-*Pbn*2$_1$) type Li_2MnSiO_4 sample had been prepared through hydrothermal method. The DFT calculations also reveal that the denser *Pmn*2$_1$ polymorph can be obtained by high-pressure / high-temperature treatment from the other polymorphs or their mixtures [44].

^{6}Li MAS NMR spectroscopic combined with DFT calculations was used to study the structural differences among various polymorphs of Li_2MSiO_4 (*M* = Mn, Fe, Zn). Results show that the fully lithiated Li_2MSiO_4, delithiated $LiMSiO_4$ and $MSiO_4$ are semiconducting and the band gap of Li_2MSiO_4 decreases while extracting lithium ions [96, 97]. The Si-O bonds remain almost unchanged during the lithiation-delithiation for all polymorphism, which contribute significantly to the structural stability [86]. Comparisons exhibit a more promising role of monoclinic *P*2$_1$/*n* configuration. The corresponding fully delithiated $MSiO_4$ attained better stability due to high-spin state from M^{2+} to M^{3+} and to M^{4+} ions [48]. Different from the counterpart of $LiMPO_4$, the potentials of Li_2MSiO_4 are largely increased due to higher valence state of M^{3+}/M^{4+} redox couple [207] and Li^+ conduction exhibits a two-dimensional anisotropic character [19].

Kokalj *et al.* predicted by DFT calculations that it might be possible to obtain a stable material with > 1 Li^+ / f.u. by using $Li_2Mn_xFe_{1-x}SiO_4$ solid solution. The voltage required is lower by 0.7 V than that for the pure Fe counterpart [202]. However, Larsson *et al.* argued that when the ratio of Mn substitution lowered to 12.5%, the structural distortion and high voltage would destruct the feasibility of this design [208].

Kalantarian *et al.* pointed out by DFT calculations that β_I-Li_2MnSiO_4 (*Pmn*2$_1$) should have better electrochemical properties, even after 2 Li^+ / f.u. extraction [203]. The insertion / extraction mechanism has been put into relation with the

voltage-capacity behaviour by considering a diffusion model. They also related voltage behaviour to relevant quantities such as reaction energy, Li^+ diffusion coefficient and particle size, so suggesting some strategies for optimizing materials [204]. $Li_2M_{0.5}N_{0.5}SiO_4$ (*M*, *N* = Mn, Fe, Co, Ni) compounds with $Pmn2_1$ structure were studied by DFT using GGA (+ U^{SIC}) and LSDA (+ U^{SIC}) methods. Mixed compounds score better than pure materials, except for Fe-Mn in comparison with Fe. Considering both electron conductivity and theoretical lithiation-delithiation reaction voltage, the best properties are showed by Fe-Ni, Mn-Ni, Fe-Co and Mn-Co, in descending order. Fe-Ni is theoretically the most promising material. Based on gravimetric specific energy, these materials are sorted as: Mn-Fe, Fe, Mn, Mn-Ni, Fe-Co, Mn-Co, Fe-Ni, Co, Co-Ni and Ni, in ascending order (Fig. 6) [205].

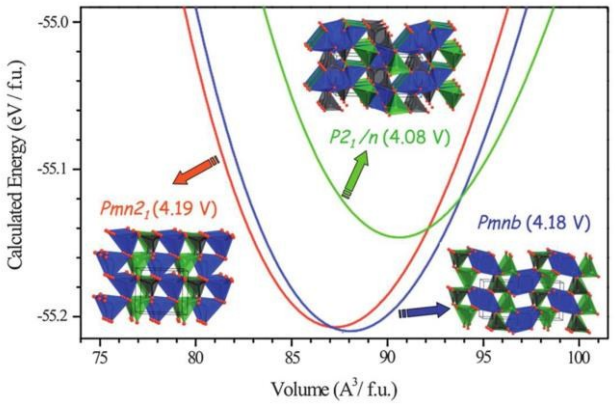

Figure 5: Calculated total energy *vs.* volume curves of Li_2MnSiO_4 polymorphs; $Pmn2_1$ (red), *Pmnb* (blue) and $P2_1/n$ (green). Calculated average voltage for the 2 electron process is given in parentheses [44, 209].

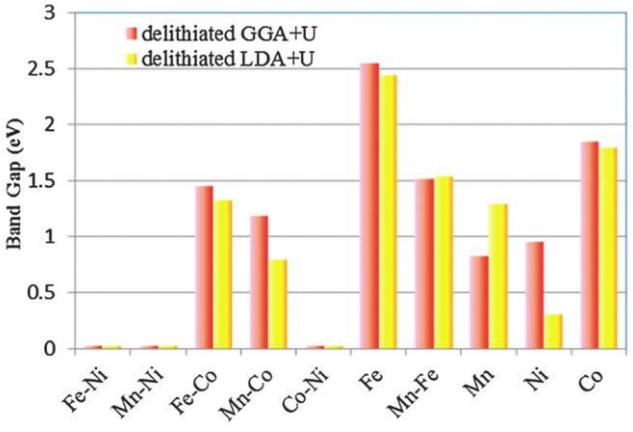

Figure 6: Band gaps for delithiated states of $Li_2M_{0.5}N_{0.5}SiO_4$ (*M*, *N* = Mn, Fe, Co, Ni) calculated *via* GGA/LSDA + U^{SIC} methods [205].

E. Techniques for Improving the Electrochemical Performance:

As mentioned earlier, just like $LiFePO_4$, Li_2MSiO_4 (*M* = Fe, Mn, Co, Ni) cathode materials also suffer from poor electronic conductivity and slow diffusion rate of lithium ion, which inhibit their use in higher power applications [45, 210]. To overcome these drawbacks, the following strategies were adopted: a) carbon coating; b) optimization of the particle size and morphology; and c) ion-substitution.

E. 1. Carbon Coating:

In synthesizing Li_2MSiO_4, carbon sources are often used to improve electrochemical properties, at the same time to act as buffers preventing grain growth and formation of hard agglomerates during heat treatment [142]. Generally, it works in two ways: **i) *In situ* carbon coating:** The starting precursors and carbon source are mixed and then calcinated at high temperature. This type of coating would form a thin and homogeneous carbon layer on the surface of particles and improve electrochemical properties [211]. The formed carbon can also affect the growth of particles or possibly increase impurities in the target materials. **ii) *Ex situ* carbon coating:** Carbon-free materials are prepared and then mixed up with carbon source by ball milling / grinding. Heat treatment is necessary if carbon precursor rather than carbon black is used. This type of coating has little effect on the morphology of particles and the amount of impurities [128].

Many researchers have suggested that the selected carbon precursors directly involved in the characteristics of the carbon additives, in terms of their structure, distribution and thickness coating layer, which are proportional to the performance of electrodes [212-215].

Carbon coating not only provides conductive connections among the active particles which are favourable to the electron and ion-transfer (Fig. 7a) [216], but also decreases the particle size effectively of the active materials during the heat treatment. It can shorten the diffusion path of lithium ion and also facilitate good contact among the neighbouring particles with reduction of the polarization [45, 61, 217]. Uniform carbon coating (~2 - 5 nm thickness on nano particles) increases the capacity and rate performance by providing short pathways and huge electrochemical interfaces for fast ions diffusions and transportation (Fig. 7b) [133, 218, 219]. Various carbon precursors directly affected the electrical conductivity of the carbon, which support to improve the electrochemical performance of Li_2MSiO_4/C cathode materials [136, 220]. Increased sp^2-coordinated carbon promised better electrochemical performance [221-223]. Functional structure or ring forming structure of organic precursor has attracted considerable attention as carbon source for electrodes [212, 221, 222].

If aggregated carbon has too much content, it would block the pathway for electrolyte percolation. Hence the ionic conduction is blocked [224]. The total amount of impurities increases with the carbon contents, *i.e.* the content of electrochemically active Li_2MSiO_4 decreases with increasing of carbon content.

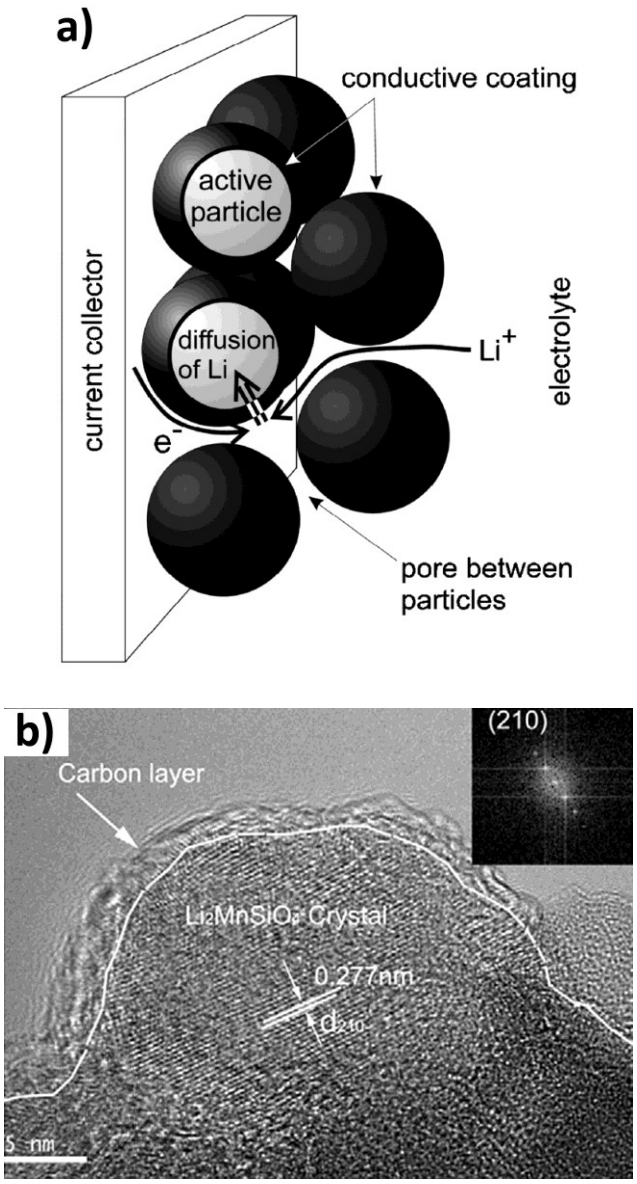

Figure 7: a) Schematic presentation of electron and ion transport in a carbon-coated cathode material [216]; b) uniform thickness of carbon coating on a Li_2MSiO_4 particle [133].

Until now, many carbon sources have been used in synthesizing Li_2MSiO_4 cathode materials, such as carbon nanosphere (CNS) [187], carbon nanotubes (CNTs) [159], reduced graphene oxide (rGO) [127], graphene oxide (GO) [125], PEG-600 [125], cellulose acetate [125], adipic acid [225], acetylene black or Ketjen black [73, 160], sucrose [20, 114, 128, 130, 131, 136, 139, 158, 170, 171, 180, 188, 212, 226-229], cellulose acetate [158], acetylene black [73, 109, 118, 132, 200, 226, 229-232], cellulose [108], polyethylene-poly (ethylene glycol) [125, 141, 153, 233], ascorbic acid [56, 156], citric acid [41, 56, 63, 82, 132, 141, 191, 216, 227, 233-236], corn starch [84, 166], glucose [62, 81, 118, 125, 183, 187, 212, 237], carbon nano sheet / tube [187, 238-241], graphene [125, 127], pyromellitic acid [135, 242], P123 polymer[243], carbon black [24, 106, 113, 134, 147, 148, 153, 187, 188, 244, 245], polyacrylonitrile [189], tartaric acid [80], adipic acid [137, 138, 160, 162, 246], pitch [81, 122] and phenolic resin [211].

Li_2MnSiO_4 *via* a sol-gel technique using 2.1 wt.% sucrose showed higher cyclic performce than that using 5.9 wt.% content [235]. Li_2MnSiO_4 *via* a sol-gel technique using 0.2 mol% adipic acid (act as carbon source and chelating agent) exhibited a better discharge capacity of 113 $mA{\cdot}h{\cdot}g^{-1}$ than that using 0.2 mol% content (58 $mA{\cdot}h{\cdot}g^{-1}$) [138]. Carbon suppression to crystallites and connecting with pores in Li_2MnSiO_4/C resulted in a carbon-coated compound. It showed a high discharge capacity of 275.2 $mA{\cdot}h{\cdot}g^{-1}$ than that in an uncoated Li_2MnSiO_4 (178.3 $mA{\cdot}h{\cdot}g^{-1}$) [136].

Li_2MnSiO_4/C *via* a combustion method using 0 wt.%, 10 wt.% and 20 wt.% of acetylene black exhibited the discharge capacity of 2 $mA{\cdot}h{\cdot}g^{-1}$, 128 $mA{\cdot}h{\cdot}g^{-1}$ and 164 $mA{\cdot}h{\cdot}g^{-1}$ respectively [142].

Graphitized carbons afford better electrochemical performance than the non-graphitized. Li_2MnSiO_4/C/graphene composite was prepared using carbon sources like polyethylene glycol 600, glucose, cellulose acetate and graphene oxide. It exhibited an initial discharge capacity of 215.3 $mA{\cdot}h{\cdot}g^{-1}$ at 0.05 C. The 3D nest-like carbon network and carbon layer are favourable for improving the capability and cycling stability [125].

E. 2. Optimization of the Particle Size and Morphology:

As per diffusion formula $t = L^2 / 2D$ (where t is the diffusion time, L the diffusion distance and D the diffusion coefficient), the rate of electrochemical performance increases with the reducing of particle size. Porous structure shortens significantly the diffusion time of Li^+ in Li_2MSiO_4 cathode materials [247, 248]. Nano-sphere particles make for increasing the tap density of cathodes, because the larger size of the secondary particles provides a denser packing, while the smaller size of the primary particles improves the Li^+ and electron conduction [171].

Li_2MnSiO_4 particles exhibited an uniform spherical shape and a size around 50 nm coated with a carbon / graphene layer (Fig. 8a) [125]. Nano spherical Li_2MnSiO_4 (20 - 30 nm) was synthesized by using a chelating agent (adipic acid). It exhibited an initial discharge capacity of ~161 $mA{\cdot}h{\cdot}g^{-1}$ and was stabled up to 50 cycles [137].

The 20 nm thin flower-like morphology with flake margin of petals formed (Fig. 8b) in Li_2MnSiO_4 during the nucleation growth in the presence of water under optimized hydrothermal treatment. The resultant exhibited electrochemical stability of ~125 $mA{\cdot}h{\cdot}g^{-1}$ due to its large surface area, unique morphology and high interconnections among the nearest neighbouring particles [116].

Large amount of pores in mesopore and macropore structures (also in hierarchical pores structure) influence greatly cycling behaviors, resulted in the discharge capacity of 275.2 $mA{\cdot}h{\cdot}g^{-1}$ in Li_2MnSiO_4/C and 163 $mA{\cdot}h{\cdot}g^{-1}$ in Li_2FeSiO_4/C at 0.06 C. Current penetrating electrolyte through porous structure was benefit for promoting Li^+ transportation [133, 136, 166, 178, 249]. Honeycomb-like $Li_{1.8}MnSO_4$ with mesopores (6 - 8 nm) was produced by decomposing raw materials at high

temperature (to release CO_2 and H_2O), which exhibited a discharge capacity of 110.9 mA·h·g^{-1} [168].

$Li_2MnSiO_4/C/V_2O_5$ in which Li_2MnSiO_4/C nano-particles adhered by V_2O_5 nano-wires exhibited a high discharge capacity of 277 mA·h·g^{-1} (1.66 Li^+ extracted LMS) at 0.1 C, because V_2O_5 nano-wires suppressed the dissolution of manganese and protected Li_2MnSiO_4 from corrosive reaction with the electrolyte [195].

Li_2MnSiO_4 with a hierarchical structure (200 - 400 nm, Fig. 8c) was prepared *via* a supercritical fluid process using oleic acid as a surfactant. It exhibited an initial discharge capacity of 283 mA·h·g^{-1} (1.7 Li^+ extracted LMS). The suitable particles size and the special structure made nearly 2 Li^+ extraction.

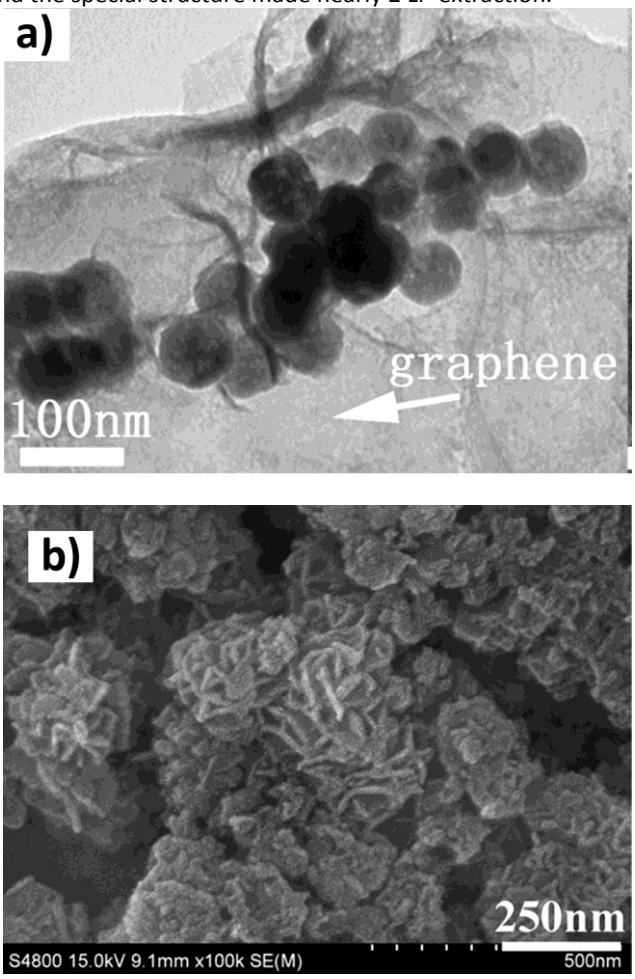

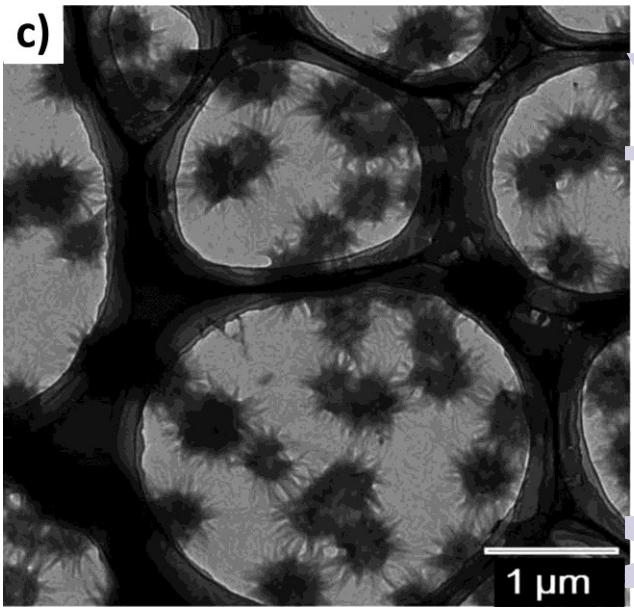

Figure 8: a) TEM of Li_2MnSiO_4 particles exhibiting an uniform spherical shape and a size around 50 nm coated with a carbon / graphene layer [125]; b) SEM of Li_2MnSiO_4 thin flowers with a flake-type petal [116]; c) TEM of Li_2MnSiO_4 particles with a hierarchical structure [250].

E. 3. Cation-Substitution:

Aliovalent / isovalent cation subsitution is often employed to improve the electrochemical performance of polyanion compounds by the alteration of cell / particle sizes of cathode materials [169, 251]. The aliovalent ion substitution is more effective [252-254] and can induce defects (vacancies or interstitials) in the lattice by charge compensation to enhance the conductivity [19, 56, 169, 255]. [252-254]High atomic percentage of aliovalent (Al^{3+}, Zr^{4+} and Nb^{5+}) substitution was reported to reduce the lithium miscibility gap and increase the phase transformation kinetics [256, 257]. But theoretical study on energetic ground proved that polyanion is not tolerant to aliovalent substitution on neither Li^+ nor M^{2+} sites [258]. Doping of aliovalent cation is still under debate [251, 258-261].

The substitution of Mn^{2+} by Cr^{3+} in $Li_2(Mn_{1-x}Cr_x)SiO_4$ / carbon nano-fiber composites (x = 0.03, 0.06 and 0.1) increased crystal unit cell volumes. The crystalline structure was prevented from collapsing and the structural stability was improved during charge / discharge cycles. The $Li_2(Mn_{0.94}Cr_{0.06})SiO_4$ exhibited a discharge capacity of 314 mA·h·g^{-1} and an improved cycling behavior due to the maximum unit cell volume [64].

The substitution of Mn^{2+} by Ti^{4+} in $Li_2(Mn_{1-x}Ti_x)SiO_4$ (x = 0, 0.06, 0.1 and 0.2) led slightly to a shrinkage of volume, due to the smaller ionic radius of Ti^{4+} than that of Mn^{2+}. Particles had smaller size, better mono-dispersion and larger specific areas compared to the pristine Li_2MnSiO_4. $Li_2(Mn_{0.8}Ti_{0.2})SiO_4$ showed good cycling performance and maintained the capacity around 100 mA·h·g^{-1} after 50 cycles (Fig. 9a) [196].

After substitution of trivalent ions like Ga^{3+}, Al^{3+} and Mg^{2+} in Li_2MnSiO_4, small intensity peaks were found in the region

Li/Mn sites. But the substitution didn't affect the structure arrangement. Only Ga^{3+} led to a better charge / discharge capacity (Fig. 9b) and exhibited an effect on well-dispersed nano-particle formation [56]. If substitution was on Si site, charge compensation could be achieved through the creation of Li^+ interstitials [19].

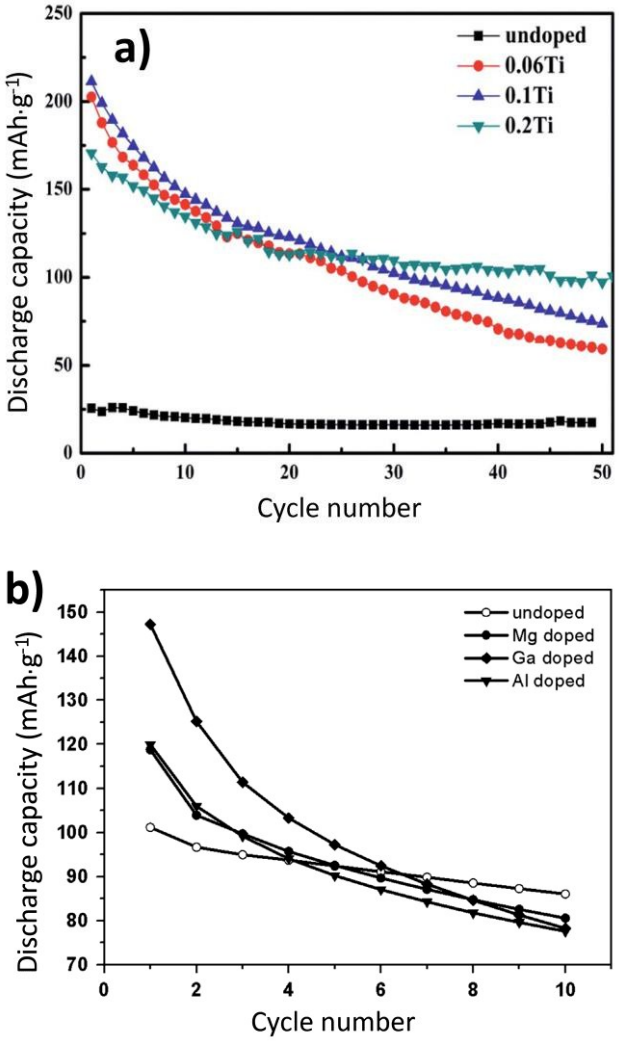

Figure 9: a) Cyclic performance of $Li_2Mn_{1-x}Ti_xSiO_4$ (x = 0, 0.06, 0.1 and 0.2) [262]; b) Cyclic Performance of Mg^{2+}, Ga^{3+} and Al^{3+} substituted Li_2MnSiO_4 [263].

The Li_2FeSiO_4 suffers low electronic conductivity and slow Li^+ diffusion. Substitution of iron with other transition metals is a possible solution to the problem. At the same time, the initial structure of Li_2MnSiO_4 is progressively amorphized during delithiation, which leads to the poor stability during cycles. In order to combine the high discharge capacity of Li_2MnSiO_4 with the high cycling stability of Li_2FeSiO_4, partial substitution of Fe^{2+} with Mn^{2+} was employed [47, 202, 233]. In this way, substitution of Fe^{2+} by Mn^{2+} which undergoes a $2^+ \rightarrow 4^+$ transition can facilitate a "> 1 electron redox reaction" through the following reaction with the removal of up to 2 Li^+, resulting in a capacity increase from 170 mA·h·g^{-1} to 340 mA·h·g^{-1} [264].

$Li^+_2(Fe^{2+}_{1-x}Mn^{2+}_x)SiO_4 \leftrightarrow Li^+_{1-x}(Fe^{3+}_{1-x}Mn^{4+}_x)SiO_4 + (1 + x)Li^+ + (1 + x)e^-$

The substitution of Fe^{2+} by Mn^{2+} in $Li_2(Fe_{1-x}Mn_x)SiO_4$ (x = 0, 0.03, 0.1, 0.2 and 0.3) through a solution route led $Li_2(Fe_{0.9}Mn_{0.1})SiO_4/C$ to exhibit an initial discharge capacity of 158.1 mA·h·g^{-1} (～0.95 Li^+ extracted LFS) with a capacity retention of 94.3% after 30 cycles [114].

The substitution of Mn^{2+} by Fe^{2+} in $Li_2(Mn_{1-x}Fe_x)SiO_4/C$ ($0 \leq x \leq 0.8$) *via* a spray pyrolysis / ball milling / annealing route led $Li_2(Mn_{0.5}Fe_{0.5})SiO_4/C$ to exhibit an initial discharge capacity of 149 mA·h·g^{-1} (～0.9 Li^+ extracted LFS) at 1 C [109]. In contrast, the substitution of Fe^{2+} by Mn^{2+} in $Li_2(Fe_{1-x}Mn_x)SiO_4$ (x = 0, 0.3, 0.5, 0.7, 1) led to a discharge capacity with only 61.4% retention after 50 cycles [113]. The Mn-substituted materials exhibited higher redox potential and higher initial discharge capacity but suffered in poor cycling performance and electrochemical reversibility. It might be due to the structural stability and electronic conductivity. The $Li_2(Fe_{0.8}Mn_{0.2})SiO_4$ showed good reversibility and exhibited an initial discharge capacity of 230.1 mA·h·g^{-1} (～1.4 Li^+ extracted LFS) at 0.1 C and retained 162 mA·h·g^{-1} after 20 cycles.

Other efforts involve of replacing O by N [265], substituting polyanion SiO_4 by AsO_4 [266], BO_3 [267], VO_4 [268], and doping trivalent Al and Ga on Si site [19].

F. Conclusions:

The pursuit of effective cathode materials in LIBs is a challenge for congregate current / future energy storage requirements. The lithium transition-metal orthosilicate Li_2MSiO_4 (*M* = Mn, Fe, Co, Ni…) should be paid more attention because it has a high theoretical capacity (～330 mA·h·g^{-1}) with a possible 2 Li^+ extraction per formula unit. In the present perspective, an attempt has been made to review Li_2MSiO_4 materials on the polymorphism of structure, synthesis methods and improving techniques for electrochemical performance.

The stable Li_2MSiO_4 polymorphs include high temperature monoclinic γ_o / γ_s ($P2_1/n$), high temperature orthorhombic γ_{II} (*Pmna, Pmnb, Cmma*), low temperature orthorhombic β_I ($Pbn2_1$, $Pna2_1$) and β_{II} ($Pmn2_1$), which are influenced by synthesis conditions and electrochemical behaviors. The metastable monoclinic P_n-Li_2MnSiO_4 would convert to the β_{II} structure ($Pmn2_1$) above 370 °C. The densest β_{II} ($Pmn2_1$) polymorph attained the best electrochemical performance due to its special structure. It can be prepared from other less-dense polymorphs, by controlling temperature, pressure and/or electrochemical process.

Once materials amorphization or collapse were inhibited during lithium ions insertion / extraction from host lattice, the reversible structural change and good cycling performance would attain. Hence, it is suggested that the ion-substitution for stabilizing the structures, is an effective way to achieve high-capacity Li_2MSiO_4 materials. Carbon-coating and optimization of the particle size / morphology are also applied as the exterior modifying methods to enhance electrochemical performance. Thus understanding the relationship among the

polymorph structure, synthesis and phase transition in Li_2MSiO_4 is the most important.

F. Acknowledgements: The authors gratefully thank Mr. Z.-S. Gao, Mr. D. Chen, Mr. J. Li, Ms. G.-G. Zhao, Mr. J.-H. Liu and Ms. H.-F. Zhang in our group. This work was supported by Postdoctoral Research Award Foundation of Wuhan University of Technology (WUT), and Open Research Foundation of State Key Laboratory of Advanced Technology for Materials Synthesis and Processing, WUT, China (Grant Nos. 2014-KF-6 & 2015-KF-4).

References:

1. K. Kang, Y. S. Meng, J. Breger, C. P. Grey and G. Ceder, *Science*, 2006, **311**, 977-980.
2. S. Nishimura, G. Kobayashi, K. Ohoyama, R. Kanno, M. Yashima and A. Yamada, *Nat. Mater*., 2008, **7**, 707-711.
3. P. Gibot, M. Casas-Cabanas, L. Laffont, S. Levasseur, P. Carlach, S. Hamelet, J.-M. Tarascon and C. Masquelier, *Nat. Mater*., 2008, **7**, 741-747.
4. D. O. Energy, U. S. A, I. N. E. E. Laboratory and L. Bechtel Bwxt Idaho, *Freedom CAR Battery Test Manual for Power-Assist Hybrid Electric Vehicles*, October 2003.
5. S.-W. Kim, T. H. Han, J. Kim, H. Gwon, H.-S. Moon, S.-W. Kang, S. O. Kim and K. Kang, *ACS Nano.*, 2009, **3**, 1085-1090.
6. D. Andre, S.-J. Kim, P. Lamp, S. F. Lux, F. Maglia, O. Paschos and B. Stiaszny, *J. Mater. Chem. A.,* 2015, **3**, 6709-6732.
7. A. K. Padhi, K. S. Nanjundaswamy and J. B. Goodenough, *J. Electrochem. Soc.*, 1997, **144**, 1188-1194.
8. A. K. Padhi, K. S. Nanjundaswamy, C. Masquelier, S. Okada and J. Goodenough, *J. Electrochem. Soc.,* 1997, **144**, 1609-1613.
9. A. Yamada, S. C. Chung and K. Hinokuma, *J. Electrochem. Soc.*, 2001, **148**, A224-A229.
10. S.-W. Kim, J. Kim, H. Gwon and K. Kang, *J. Electrochem. Soc.*, 2009, **156**, A635-A638.
11. H. Gwon, D.-H. Seo, S.-W. Kim, J. Kim and K. Kang, *Adv. Funct. Mater.*, 2009, **19**, 3285-3292.
12. D.-H. Seo, H. Gwon, S.-W. Kim, J. Kim and K. Kang, *Chem. Mater.*, 2010, **22**, 518-523.
13. J. Kim, D.-H. Seo, S.-W. Kim, Y.-U. Parka, K. Kang and S. Affiliations, *Chem. Commun.,* 2010, **46**, 1305-1307.
14. Y.-U. Park, J. Kim, H. Gwon, D.-H. Seo, S.-W. Kim and K. Kang, *Chem. Mater.,*2010, **22**, 2573-2581.
15. W. Sun, C. Deng, H. Hao, Y. Kang and Y. Si, *Mater. Lett.*, 2013, **93**, 49-51.
16. Z. Zhao, X. Si, X. Liu, L. He and X. Liang, *Hydrometallurgy*, 2013, **133**, 75-83.
17. J. Song, L. Wang, G. Shao, M. Shi, Z. Ma, G. Wang, W. Song, S. Liuab and C. Wanga, *Phys. Chem. Chem. Phys.*, 2014, **16**, 7728-7733.
18. M. Arroyo-de Dompablo, M. Armand, J. Tarascon and U. Amador, *Electrochem. Commun.*, 2006, **8**, 1292-1298.
19. N. Kuganathan and M. S. Islam, *Chem. Mater.,* 2009, **21**, 5196-5202.
20. L. Qu, S. Fang, Z. Zhang, L. Yang and S.-i. Hirano, *Mater. Lett.*, 2013, **108**, 1-4.
21. C. Zhang, Z. Chen and J. Li, *Chem. Phys. Lett.*, 2013, **580**, 115-119.
22. J. Cui, C. Qing, Q. Zhang, C. Su, X. Wang, B. Yang and X. Huang, *Ionics*, 2013, **20**, 23-28.
23. A. Nytén, A. Abouimrane, M. Armand, T. Gustafsson and J. O. Thomas, *Electrochem. Commun.*, 2005, **7**, 156-160.
24. M. Reynaud. Ph.D Thesis, "*Design of new sulfate-based positive electrode materials for Li- and Na-ion batteries*", Universite de Picardie Jules Verne**,** 2014.
25. D. Chen, G. Q. Shao, B. Li, G. G. Zhao, J. Li, J. H. Liu, Z. S. Gao and H. F. Zhang, *Electrochim. Act*, 2014, **147**, 663-668.
26. S. Ferrari, D. Capsoni, S. Casino, M. Destro, Gerbaldi and M. Bini, *Phys. Chem. Chem. Phys.*, 2014, **16**, 10353-10366.
27. N. Recham, J. N. Chotard, L. Dupont, C. Delacourt, W. Walker, M. Armand and J. M. Tarascon, *Nat. Mater.*, 2010, **9**, 68-74.
28. N. Recham, M. Casas-Cabanas, J. Cabana, C. P. Grey, J.-C. Jumas, L. Dupont, M. Armand and J.-M. Tarascon, *Chem. Mater.,*2008, **20**, 6798-6809.
29. V. Legagneur, Y. An, A. Mosbah, R. Portal, A. L. G. L. Salle, A. Verbaere, D. Guyomard and Y. Piffard, *Solid State Ionics*, 2001, **139**, 37-46.
30. A. Abouimarne, M. Armand and N. Ravet, *J. Electrochem. Soc.,* 2003, 15-22.
31. Y. Z. Donga, Y. M. Zhaoa, Z. D. Shib, X. N. Anc, P. Fua and L. Chen, *Electrochim. Act*, 2008, **53**, 2339-2345.
32. A. Yamada, N. Iwane, Y. Harada, S. Nishimura, Y. Koyama and I. Tanaka, *Adv. Mater.*, 2010, **22**, 3583-3587.
33. Y. Koyama, I. Tanaka, N. Iwane, S. Nishimura and A. Yamada, *The 15th international meeting on Lithium Battries, Monteal, Canada,* 2010.
34. Q. Zhang, Y. Zhao, C. Su and L. Li, *Recent Pat. Nanotech*., 2011, **9**, 225-233.
35. B. L. Ellis, K. T. Lee and L. F. Nazar, *Chem. Mater.*, 2010, **22**, 691-714.
36. C. Lyness, B. Delobel, A. R. Armstronga and P. G. Bruce, *Chem. Commun.*, 2007, 4890-4892.
37. R. Dominko, M. Bele, M. Gaberšček, A. Meden, M. Remškar and J. Jamnik, *Electrochem. Commun.*, 2006, **8**, 217-222.
38. M. S. Islam, R. Dominko, C. Masquelier, C. Sirisopanaporn, A. R. Armstrong and P. G. Bruce, *J. Mater. Chem.*, 2011, **21**, 9811-9818.
39. P. Larsson, R. Ahuja, A. Nytén and J. O. Thomas, *Electrochem. Commun.*, 2006, **8**, 797-800.
40. R. C. Longo, K. Xiong and K. Cho, *ECS Trans.*, 2012, **41**, 75-85.
41. C. Deng, S. Zhang, B. L. Fu, S. Y. Yang and L. Ma, *Mater. Chem. Phys.*, 2010, **120**, 14-17.
42. R. Dominko, I. Arčon, A. Kodre, D. Hanžel and M. Gaberšček, *J. Power Sources*, 2009, **189**, 51-58.
43. M. Arroyo-de Dompablo, U. Amador, J. M. Gallardo-Amores, E. Morán, H. Ehrenberg, L. Dupont and R. Dominko, *J. Power Sources*, 2009, **189**, 638-642.

44. M. Arroyo-de Dompablo, R. Dominko, J. M. Gallardo-Amores, L. Dupont, G. Mali, H. Ehrenberg, J. Jamnik and E. Moran, *Chem. Mater.*, 2008, **20**, 5574-5584.
45. R. Dominko, *J. Power Sources*, 2008, **184**, 462-468.
46. V. Srinivasan and J. Newman, *J. Electrochem. Soc.*, 2004, **151**, A1517-A1529.
47. Z. Gong, Y. Li and Y. Yang, *J. Power Sources*, 2007, **174**, 524-527.
48. G. Zhong, Y. Li, P. Yan, Z. Liu, M. Xie and H. Lin, *J. Phys. Chem. C*, 2010, **114**, 3693-3700.
49. G. He, G. Popov and L. F. Nazar, *Chem. Mater.*, 2013, **25**, 1024-1031.
50. J.-M. Tarascon and M. Armand, *Nature*, 2001, **414**, 359-367.
51. M. Armand and J.-M. Tarascon, *Nature*, 2008, **451**, 652-657.
52. J. B. Goodenough and Y. Kim, *J. Power Sources*, 2011, **196**, 6688-6694.
53. J. B. Goodenough, *Acc. Chem. Res.*, 2013, **46,** 1053-1061.
54. H.-K. Song, K. T. Lee, M. G. Kim, L. F. Nazar and J. Cho, *Adv. Funct. Mater.*, 2010, **20**, 3818-3834.
55. D. Rangappa, K. D. Murukanahally, T. Tomai, A. Unemoto and I. Honma, *Nano Lett.*, 2012, **12**, 1146-1151.
56. L. L. Zhang, S. Duan, X. L. Yang, G. Peng, G. Liang, Y. H. Huang, Y. Jiang, S. B. Ni and M. Li, *ACS Appl. Mater. Inter*., 2013, **5**, 12304-12309.
57. J. Yang, L. Hu, J. Zheng, D. He, L. Tian, S. Mu and F. Pan, *J. Mater. Chem. A,*2015, **3**, 9601-9608.
58. R. Dominko, C. Sirisopanaporn, C. Masquelier, D. Hanzel, I. Arcon and M. Gaberscek, *J. Electrochem. Soc.,* 2010, **157**, A1309-A1316.
59. C. Deng, S. Zhang, S. Y. Yang, Y. Gao, B. Wu, L. Ma, B. L. Fu, Q. Wu and F. L. Liu, *J. Phys. Chem. C***,** 2011, **115**, 15048-15056.
60. S. Zhang, C. Deng, B. L. Fu, S. Y. Yang and L. Ma, *Electrochim. Acta*,2010, **55**, 8482-8489.
61. S. Zhang, C. Deng, B. L. Fu, S. Y. Yang and L. Ma, *J. Electroanal. Chem.*, 2010, **644**, 150-154.
62. H. Yamashita, S. Ishihara, T. Ogami and T. Sujuki, *J. Taiheiyo Cem. Corp. (Japan),* 2013, 165, 42-52.
63. H. Hao, J. Wang, J. Liu, T. Huang and A. Yu, *J. Power Sources*, 2012, **210**, 397-401.
64. S. Zhang, Z. Lin, L. Ji, Y. Li, G. Xu, L. Xue, S. Li, Y. Lu, O. Toprakcia and X. Zhang, *J. Mater. Chem.*, 2012, **22**, 14661-14666.
65. L.-L. Zhang, S. Duan, X.-L. Yang, G. Liang, Y.-H. Huang, X.-Z. Cao, J. Yang, M. Li, M. C. Croft and C. Lewis, *J. Power Sources*, 2015, **274**, 194-202.
66. C. H. Jiang, S. X. Dou, H. K. Liu, M. Ichihara and H. S. Zhou, *J. Power Sources*, 2007, **172**, 410-415.
67. J.-M. Chen, Y.-D. Cho, C.-L. Hsiao and G. T.-K. Fey, *J. Power Sources*, 2009, **189**, 279-287.
68. J. Lee and A. S. Teja, *J. Supercrit. Fluids.*, 2005, **35**, 83-90.
69. V. Borgel, E. Markevich, D. Aurbach, G. Semrau and M. Schmidt, *J. Power Sources*, 2009, **189**, 331-336.
70. Z. Li, D. Zhang and F. Yang, *J. Mater. Sci.*, 2009, **44**, 2435-2443.
71. S. Nieto-Ramos and M. S. Tomar, *Int. J. Hydrogen Energy*,2001, **26**, 159-163.
72. J. F. Whitacre, K. Zaghib, W. C. West and B. V. Ratnakumar, *J. Power Sources*, 2008, **177**, 528-536.
73. K. C. Kam, T. Gustafsson and J. O. Thomas, *Solid State Ionics*, 2011, **192**, 356-359.
74. H. Liu, L. J. Fu, H. P. Zhang, J. Gao, C. Li, Y. P. Wu and H. Q. Wu, *Electrochem. Solid-State Lett.*,2006, **9**, A529-A233.
75. Z. Chen, Y. Qin, K. Amine and Y. K. Sun, *J. Mater Chem.*, 2010, 2, 7606-7612.
76. W. Chen, M. Lan, D. Zhu, C. Wang, S. Xue, C. Yang, Z. Li, J. Zhang and L. Mi, *RSC Adv.*, 2013, **3**, 408.
77. P. Zuo, T. Wang, G. Cheng, C. Du, Y. Ma, X. Cheng and G. Yin, *J. Solid State Electrochem.*, 2013, **17**, 1955-1959.
78. L.-m. Li, H.-j. Guo, X.-h. Li, Z.-x. Wang, W.-j. Peng, K.-x. Xiang and X. Cao, *J. Power Sources*, 2009, **189**, 45-50.
79. X. Wu, X. Jiang, Q. Huo and Y. Zhang, *Electrochim. Acta*, 2012, **80**, 50-55.
80. Z. Zheng, Y. Wang, A. Zhang, T. Zhang, F. Cheng, Z. Tao and J. Chen, *J. Power Sources*,2012, **198**, 229-23
81. X. Huang, X. Li, H. Wang, Z. Pan, M. Qu and Z. Yu, *Solid State Ionics*, 2010, **181**, 1451-1455.
82. X.-Y. Fan, Y. Li, J.-J. Wang, L. Gou, P. Zhao, D.-L. Li, L. Huang and S.-G. Sun, *J. Alloys Compd.*, 2010, **493**, 77-80.
83. H. Duncan, A. Kondamreddy, P. H. J. Mercier, Y. Le Page, Y. Abu-Lebdeh, M. Couillard, P. S. Whitfield and I. J. Davidson, *Chem. Mater.*, 2011, **23**, 5446-5456.
84. N. Wagner, A.-M. Svensson and F. Vullum-Bruer, *Solid State Ionics*, 2015, **276**, 26-32.
85. A.R. West and F. P. Glasser, *J. Solid State Chem.*, 1972, **4**, 20-28.
86. A. R. Armstrong, N. Kuganathan, M. S. Islam and P. G. Bruce, *J. Am. Chem. Soc.*, 2011, **133**, 13031-13035.
87. G. Quoirin, F. Taulelle, L. Dupont and C. Masquelier, *Abstract 98.*, 2007.
88. G. Quoirin, Ph.D. Thesis, Universite de Picardie Jules Verne, Amiens, France, 2007.
89. G. Quoirin, J. M. Tarascon, C. Masquelier, C. Delacourt, P. Poizot and F. Taulelle, *World Patent WO2008/107571 A2*, 2008.
90. C. Eames, A. R. Armstrong, P. G. Bruce and M. S. Islam, *Chem. Mater.*, 2012, **24**, 2155-2161.
91. A. Saracibar, A. Van der Ven and M. Arroyo-de Dompablo, *Chem. Mater.*, 2012, **24**, 495-503.
92. H. Yamaguchi and K. Akatsuka, *Acta. Cryst.*, 1979, **B35**, 2680-2682.
93. A. Boulineau, C. Sirisopanaporn, R. Dominko, A. R. Armstrong, P. G. Bruce and C. Masquelier, *Dalton T.*, 2010, **39**, 6310-6316.
94. A. Yamada, *Oral presentation and personal communication, LiBD meeting, Arcachon, France*, 2009**.**
95. S.-I. Nishimura, S. Hayase, R. Kanno, M. Yashima, Nakayama and A. Yamada, *J. Am. Chem. Soc.*, 2008, **130**, 13212-13213.
96. G. Mali, M. Rangus, C. Sirisopanaporn and R. Dominko, *Solid State Nucl. Magn. Reson.*, 2012, **4** 33-41.
97. G. Mali, A. Meden and R. Dominkoa, *Chem. Commun.*, 2010, **46**, 3306-3308.

98. C. Sirisopanaporn, R. Dominko, C. Masquelier, A. R. Armstrong, G. Mali and P. G. Bruce, *J. Mater. Chem.*, 2011, **21**, 17823-17831.
99. A. Nyten, S. Kamali, L. Haggstrom, T. Gustafsson and J. O. Thomas, *J. Mater. Chem.*, 2006, **16**, 2266-2272.
100. C. Sirisopanaporn, C. Masquelier, P. G. Bruce, A. R. Armstrong and R. Dominko, *J. Am. Chem. Soc.*, 2011, **133**, 1263-1265.
101. A. R. Armstrong, C. Sirisopanaporn, P. Adamson, J. Billaud, R. Dominko, C. Masquelier and P. G. Bruce, *Z. Anorg. Allg. Chem.*, 2014, **640**, 1043-1049.
102. R. Chen, R. Heinzmann, S. Mangold, V. S. K. Chakravadhanula, H. Hahn and S. Indris, *J. Phys. Chem. C*, 2013, **117**, 884-893.
103. C. Sirisopanaporn, A. Boulineau, D. Hanzel, R. Dominko, B. Budic, A. R. Armstrong, P. G. Bruce and C. Masquelier, *Inorg. Chem.*, 2010, **49**, 7446-7451.
104. T. Masese, Y. Orikasa, C. d. Tassel, J. Kim, T. Minato, H. Arai, T. Mori, K. Yamamoto, Y. Kobayashi, H. Kageyama, Z. Ogumi and Y. Uchimoto, *Chem. Mater.*, 2014, **26**, 1380−1384.
105. J. Shim, S. Won, G. Park and H.-J. Sun, *Adv. Mater. Phys. Chem.*, 2012, **02**, 185-188.
106. V. V. Politaev, A. A. Petrenko, V. B. Nalbandyan, B. S. Medvedev and E. S. Shvetsova, *J. Solid State Chem.*, 2007, **180**, 1045-1050.
107. Y.-X. Li, Z.-L. Gong and Y. Yang, *J. Power Sources*, 2007, **174**, 528-532.
108. I. Belharouak, A. Abouimrane and K. Amine, *J. Phys. Chem. C*, 2009, **113**, 20733-20737.
109. B. Shao, Y. Abe and I. Taniguchi, *Powder Technol.*, 2013, **235**, 1-8.
110. S. Q. Wu, J. H. Zhang, Z. Z. Zhu and Y. Yang, *Curr. Appl. Phys*., 2007, **7**, 611-616.
111. S. Q. Wu, Z. Z. Zhu, Y. Yang and Z. F. Hou, *Comp. Mater. Sci*., 2009, **44**, 1243-1251.
112. K. M. Bui, V. A. Dinh and T. Ohno, *J. Phys. Conf. Ser.*, 2013, **454**, 1-6.
113. C. Deng, S. Zhang and S. Y. Yang, *J. Alloys Compd.*,2009, **487**, L18-L23.
114. H. Guo, X. Cao, X. Li, L. Li, X. Li, Z. Wang, W. Peng and Q. Li, *Electrochim. Acta*, 2010, **55**, 8036-8042.
115. M. Bini, S. Ferrari, D. Capsoni, C. Spreafico, C. Tealdi and P. Mustarelli, *J. Solid State Chem.*, 2013, **200**, 70-75.
116. S. Luo, M. Wang and W. Sun, *Ceram. Int.*, 2012, **38**, 4325-4329.
117. N. Yabuuchi, Y. Yamakawa, K. Yoshii and S. Komaba, *Electrochemistry*, 2010, **78**, 363-366.
118. M. Zhang, Q. Chen, Z. Xi, Y. Hou and Q. Chen, *J. Mater Sci.*, 2012, **47**, 2328-2332.
119. D. Xiao, R. M. Lianyi Shao, J. G. Miao Shui, F. Huang, K. Wu, S. Qian, D. Wang, N. Long, Y. Ren and J. Shu, *Int. J. Electrochem. Sci.*, 2013, **8**, 7581- 7590.
120. J. Yang, X. Kang, D. He, T. Peng, L. Hu and S. Mu, *J. Power Sources*, 2013, **242**, 171-178.
121. X. Huang, X. Li, H. Wang, Z. Pan, M. Qu and Z. Yu, *Electrochim. Acta*, 2010, **55**, 7362-7366.
122. X. Huang, H. Chen, S. Zhou, Y. Chen, J. Yang, Y. Ren, H. Wang, M. Qu, Z. Pan and Z. Yu, *Electrochim. Acta*, 2012, **60**, 239-243.
123. S. Zhang, Y. Li, G. Xu, S. Li, Y. Lu, O. Topracki and X. Zhang, *Soft Nanosci.Lett.,* 2012, **02**, 54-57.
124. J. Cui, C. Qing, Q. Zhang, C. Su, X. Wang, B. Yang and X. Huang, *Ionics*, 2014, **20**, 23-28.
125. H. Gong, Y. Zhu, L. Wang, D. Wei, J. Liang and Y. Qian, *J. Power Sources*, 2014, **246**, 192-197.
126. A. A. Popovich, P. A. Novikov, A. O. Silin, N. G. Razumov and W. Q. Sheng, *Russ. J. Appl. Chem.*, 2014, **87**, 1268-1273.
127. X. Wang, C. Qing, Q. Zhang, W. Fan, X. Huang, B. Yang and J. Cui, *Electrochim. Acta*, 2014, **134**, 371-376.
128. W. Liu, Y. Xu and R. Yang, *J. Alloys Compd.*, 2009, **480**, L1-L4.
129. M. Bini, S. Ferrari, C. Ferrara, M. C. Mozzati, D. Capsoni, A. J. Pell, G. Pintacuda, P. Canton and P. Mustarelli, *Sci. Rep.*, 2013, **3**, 3452.
130. L. Qu, S. Fang, L. Yang and S.-i. Hirano, *J. Power Sources*, 2014, **252**, 169-175.
131. C. Deng, Y. H. Sun, S. Zhang, H. M. Lin, Y. Gao, B. Wu, L. Ma, Y. Shang and G. Dong, *Int. J. Electrochem. Sci.*, 2012, **7**, 4559-4566.
132. X. Jiang, H. Xu, J. Liu and Y. Qian, *Mater. Lett.*, 2012, **113**, 9-12.
133. S. Liu, J. Xu, D. Li, Y. Hu, X. Liu and K. Xie, *J. Power Sources*, 2013, **232**, 258-263.
134. MinWang, M. Yang, L. Ma, X. Shen and X. Zhang, *J. Nanomater.*, 2014, **2014**, 1-6.
135. M. Świętosławski, M. Molenda, K. Furczoń and R. Dziembaj, *J. Power Sources*, 2013, **244**, 510-514.
136. F. Wang, J. Chen, C. Wang and B. Yi, *J. Electroanal. Chem.*, 2013, **688**, 123-129.
137. V. Aravindan, K. Karthikeyan, S. Ravi, S. Amaresh, W. S. Kim and Y. Lee, *J. Mater. Chem.*, 2010, **20**, 7340-7343.
138. V. Aravindan, S. Ravi, W. S. Kim, S. Y. Lee and Y. S. Lee, *J. Colloid. Interface Sci.*, 2011, **355**, 472-477.
139. B. Shao and I. Taniguchi, *Electrochim. Acta*, 2014, **128**, 156-162.
140. M. Moriya, M. Miyahara, M. Hokazono, H. Sasaki, A. Nemoto, S. Katayama, Y. Akimoto and S. i. Hirano, *J. Electrochem. Soc.*, 2013, **161**, A97-A101.
141. J.-J. Choi, S. Kim, W.-B. Im, W. Chang, B.-W. Cho, J. H. Kim, H.-L. Choi and K. Y. Chung, *J. Electroceram.*, 2013, **31**, 176-180.
142. P. Ghosh, S. Mahanty and R. N. Basu, *J. Electrochem. Soc.*, 2009, **156**, A677-A681.
143. A. R. Armstrong, C. Lyness, M. Ménétrier and P. G. Bruce, *Chem. Mater.*, 2010, **22**, 1892-1900.
144. D. Santamaria-Perez, U. Amador, J. Tortajada, R. Dominko and M. Arroyo-de Dompablo, *Inorg. Chem.*, 2012, **51**, 5779-5786.
145. M. K. Devaraju, Q. D. Truong and I. Honma, *RSC Adv.*, 2013, **3**, 20633-20638.
146. H. Gao, L. Wang, Y. Zhang, A. Zhang and Y. Song, *Powder Technol.*, 2014, **253**, 638-643.
147. M. Dahbi, S. Urbonaite and T. Gustafsson, *J. Power Sources*, 2012, **205**, 456-462.
148. H. Zhou, M.-A. Einarsrud and F. Vullum-Bruer, *Solid State Ionics*, 2012, **225**, 585-589.
149. O. Kamon-in, W. Klysubun, W. Limphirat, S. Srilomsak and N. Meethong, *Physica B Condens. Matter.*, 2013, **416**, 69-75.

150. R. J. Gummow, N. Sharma, V. K. Peterson and Y. He, *J. Solid State Chem.*, 2012, **188**, 32-37.
151. D. Lv, W. Wen, X. Huang, J. Bai, J. Mi, S. Wu and Y. Yang, *J. Mater. Chem.*, 2011, **21**, 9506-9512.
152. D. Ensling, M. Stjerndahl, A. Nyten, T. Gustafsson and J. O. Thomas, *J. Mater. Chem.*,, 2009, **19**, 82.
153. A. Nyten, M. Stjerndahl, H. Rensmo, H. Siegbahn, M. Armand, T. Gustafsson, K. Edstroma and J. O. Thomas, *J. Mater. Chem.*, 2006, **16**, 3483.
154. D.-H. Seo, H. Kim, I. Park, J. Hong and K. Kang, *Phys. Rev. B*, 2011, **84**, 220106-220101.
155. A. Kojima, T. Kojima and T. Sakai, *J. Electrochem. Soc.*, 2012, **159**, A525-A531.
156. D. M. Kempaiah, D. Rangappa and I. Honma, *Chem. Commun.*, 2012, **48**, 2698-2700.
157. C. M. Julien, A. Mauger, A. Ait-Salah, M. Massot, F. Gendron and K. Zaghib, *Ionics*, 2007, **13**, 395-411.
158. K. Zaghib, N. Ravet, M. Gauthier, F. Gendron, A. Mauger, J. B. Goodenough and C. M. Julien, *J. Power Sources*, 2006, **163**, 560-566.
159. X. Huang, H. Chen, H. Wang, S. Zhou, Y. Chen, B. Liu, J. Yang, G. Zhou, Q. Jiang, M. Qu, Z. Pan and Z. Yu, *Solid State Ionics*, 2012, **220**, 18-22.
160. K. Karthikeyan, V. Aravindan, S. B. Lee, I. C. Jang, H. H. Lim, G. J. Park, M. Yoshio and Y. S. Lee, *J. Alloys Compd.*, 2010, **504**, 224-227.
161. L.-L. Zhang, H.-B. Sun, X.-L. Yang, Y.-W. Wen, Y.-H. Huang, M. Li, G. Peng, H.-C. Tao, S.-B. Ni and G. Liang, *Electrochim. Acta*, 2015, **152**, 496-504.
162. V. Aravindan, K. Karthikeyan, J. W. Lee, S. Madhavi and Y. S. Lee, *J. Phys. D: Appl. Phys.*, 2011, **44**, 152001-152004.
163. K. Gao, C.-S. Dai, J. Lv and S.-D. Li, *J. Power Sources*, 2012, **211**, 97-102.
164. S. Thayumanasundaram, V. S. Rangasamy, J. W. Seo and J.-P. Locquet, *Ionics*, 2014, 1-7.
165. A. Nyten, S. Kamali, L. Haggstrom, T. Gustafsson and J. O. Thomas, *J. Mater. Chem.*, 2006, **16**, 2266-2272.
166. H. Zhou, M.-A. Einarsrud and F. Vullum-Bruer, *J. Power Sources*, 2013, **235**, 234-242.
167. M. Wang, M. Yang, L. Ma and X. Shen, *Chem. Phys. Lett.*, 2015, **619**, 39-43.
168. H. Wang, T. Hou, D. Sun, X. Huang, H. He, Y. Tang and Y. Liu, *J. Power Sources*, 2014, **247**, 497-502.
169. C. Deng, S. Zhang, S. Y. Yang, B. L. Fu and L. Ma., *J. Power Sources*, 2011, **196**, 386-392.
170. S. Zhang, C. Deng, H. Gao, F. L. Meng and M. Zhang, *Electrochim. Acta*, 2013, **107**, 406-412.
171. T. Muraliganth, K. R. Stroukoff and A. Manthiram, *Chem. Mater.*, 2010, **22**, 5754-5761.
172. H. Lee, S.-D. Park, J. Moon, H. Lee, K. Cho, M. Cho and S. Y. Kim, *Chem. Mater.,* 2014, **26**, 3896-3899.
173. J. Hwang, S. Park, C. Park, W. Cho and H. Jang, *Met. Mater. Int.*, 2013, **19**, 855-860.
174. J. Thomas, T. Gustafsson, L. Häggström, A. Liivat, M. Dahbi, K. Kam and D. Ensling, *A Quantum Leap Forward for Li-Ion Battery Cathodes*, 2010.
175. C.-H. Hsu, Y.-W. Shen, L.-H. Chien and P.-L. Kuo, *J. Nanopart. Res.*, 2015, **17**, 1-9.
176. J. Yang, X. Kang, L. Hu, X. Gong and S. Mu, *J. Mater. Chem. A*, 2014, **2**, 6870-6878.
177. M. Devaraju, T. Tomai and I. Honma, *Electrochim. Acta*, 2013, **109**, 75-81.
178. Y. Xu, W. Shen, A. Zhang, H. Liu and Z. Ma, *J. Mater. Chem. A*, 2014, **2**, 12982-12990.
179. L. Zhang, J. Ni, W. Wang, J. Guo and L. Li, *J. Mater. Chem. A*, 2015, **3,** 11782-11786.
180. C. Dippel, S. Krueger, R. Kloepsch, P. Niehoff, B. Hoffmann, S. Nowak, S. Passerini, M. Winter and J. Li, *Electrochim. Acta*,, 2012, **85**, 66-71.
181. A. Saracibar, Z. Wang, K. J. Carroll, Y. S. Meng and M. Arroyo-de Dompablo, *J. Mater. Chem. A*, 2015, **3**, 6004-6011.
182. M. Higuchi, K. Katayama, Y. Azuma, M. Yukawa and M. Suhara, *J. Power Sources*, 2003, **119-121**, 258-261.
183. Z. D. Peng, Y. B. Cao, G. R. Hu, K. Du, X. G. Gao and Z. W. Xiao, *Chin. Chem. Lett.,* 2009, **20**, 1000-1004.
184. Z. D. Peng, Y. B. Cao, G. R. Hu, K. Du, X. G. Gao and Z. W. Xiao, *Chin. J. Nonferrous Met.*, 2009, **19**, 1450-1454.
185. P. Tarte and R. Cahay, *Comptes Rend Hebdomadaires Des Seances De L Academie Des Sciences Serie. C*, 1970, **271**, 777.
186. I. Taniguchi, N. Fukuda and M. Konarova, *Powder Technol.*, 2008, **181**, 228-236.
187. J. Yang, X. Kang, L. Hu, X. Gong, D. He, T. Peng and S. Mu, *J. Alloys Compd.*, 2013, **572**, 158-162.
188. H.-j. Guo, K.-x. Xiang, X. Cao, X.-H. Li, Z.-x. Wang and L.-m. Li, *Trans. Nonferrous Met. Soc. China*, 2009, **19**, 166-169.
189. S. Zhang, Y. Li, G. Xu, S. Li, Y. Lu, O. Toprakci and X. Zhang, *J. Power Sources*, 2012, **213**, 10-15.
190. Z. Zhang, X. Liu, L. Wang, Y. Wu, H. Zhao and B. Chen, *Solid State Ionics*, 2015, **276**, 33-39.
191. C.-Y. Hu, J. Guo, J. Wen and Y.-X. Peng, *J. Cent. South Univ.*, 2014, **21**, 1285-1289.
192. H. Qiu, K. Zhu, H. Li, T. Li, T. Zhang, H. Yue, Y. Wei, F. Du, C. Wang, G. Chen and D. Zhang, *Carbon*, 2015, **87**, 365-373.
193. L. Qu, Y. Liu, S. Fang, L. Yang and S.-I. Hirano, *Electrochim. Acta*, 2015, **163**, 123-131.
194. C. Deng, S. Zhang, G. S. Zhao, Z. Dong, Y. Shang, Y. X. Wu and B. D. Zhao, *J. Electrochem. Soc.*, 2013, **60**, A1457-A1466.
195. J. Setoguchi, S. Kobayashi, H. Yamaguchi, C. Sakamoto and K. Akatsuka, *Mem. Osaka Kyioku Univer.* 1979, **28**, 27.
196. P. Zhang, C. H. Hu, S. Q. Wu, Z. Z. Zhu and Y. Yang, *Phys. Chem. Chem. Phys.,* 2012, **14**, 7346-7351.
197. M. Arroyo-de Dompablo, R. Dominko, J. M. Gallardo-Amores, L. Dupont, G. Mali, H. Ehrenberg, J. Jamnik and E. Moran, *Chem. Mater.*, 2008, **20**, 5574-5584.
198. M. K. Devaraju, Q. D. Truong, T. Tomai and I. Honma, *RSC Adv.*, 2014, **4**, 27452-27470.
199. X. Zeng, M. Gong, J. i. Chen and X. Zheng, *Int. Electrochem. Sci.*, 2015, **10**, 4453- 4460.
200. B. Shao and I. Taniguchi, *J. Power Sources*, 2012, **199**, 278-286.
201. T. Zhang, D. Li, Z. Tao and J. Chen, *Progress in Natural Science: Materials International*, 2013, **23**, 256-272.
202. A. Kokalj, R. Dominko, G. Mali, A. Meden, M. Gaberscek and J. Jamnik, *Chem. Mater.*, 2007, **19**, 3633-3640.

203. M. M. Kalantarian, S. Asgari and P. Mustarelli, *J. Mater. Chem. A,* 2013, **1**, 2847-2855.
204. M. M. Kalantarian, M. Oghbaei, S. Asgari, S. Ferrari, D. Capsoni and P. Mustarelli, *J. Mater. Chem. A,* 2014, **2**, 19451-19460.
205. M. M. Kalantarian, S. Asgari, D. Capsoni and P. Mustarelli, *Phys. Chem. Chem. Phys.*, 2013, **15**, 8035-8041.
206. A. Liivat and J. O. Thomas, *Solid State Ionics*, 2011, **192**, 58-64.
207. F. Zhou, M. Cococcioni, K. Kang and G. Ceder, *Electrochem. Commun.,*2004, **6**, 1144-1148.
208. P. Larsson, R. Ahuja, A. Liivat and J. O. Thomas, *Comput. Mater. Sci*, 2010, **47**, 678-684.
209. M. D. Bhatt and C. O'Dwyer, *Phys. Chem. Chem. Phys.* 2015, **17**, 4799-4844.
210. V. Aravindan, K. Karthikeyan, K. S. Kang, W. S. Yoon, W. S. Kim and Y. S. Lee, *J. Mater. Chem.*, 2011, **21**, 2470-2475.
211. D. Sun, H. Wang, P. Ding, N. Zhou, X. Huang, S. Tan and Y. Tang, *J. Power Sources,* 2013, **242**, 865-871.
212. Z.-Y. Chen, H.-l. Zhu, S. Ji, R. Fakir and V. Linkov, *Solid State Ionics*, 2008, **179**, 1810-1815.
213. Y.-D. Cho, G. T.-K. Fey and H.-M. Kao, *J. Power Sources*, 2009, **189**, 256-262.
214. J. D. Wilcox, M. M. Doeff, M. Marcinek and R. Kostecki, *J. Electrochem. Soc.*, 2007, **154**, A389-A395.
215. X. Zhi, G. Liang, L. Wang, X. Ou, L. Gao and X. Jie, *J. Alloys Compd.*, 2010, **503**, 370-374.
216. J. Moskon, R. Dominko, R. Cerc-Korosec, M. Gaberscek and J. Jamnik, *J. Power Sources*, 2007, **174**, 683-688.
217. B. Kang and G. Ceder, *Nature*, 2009, **458**, 190-193.
218. K. Saravanan, M. V. Reddy, P. Balaya, H. Gong, B. V. R. Chowdari and J. J. Vittal, *J. Mater. Chem.*, 2009, **19**, 605-610.
219. K. Saravanan, P. Balaya, M. V. Reddy, B. V. R. Chowdari and J. J. Vittal, *Energ. Environ. Sci.*, 2010, **3**, 457-464.
220. Y.-H. Nien, J. R. Carey and J.-S. Chen, *J. Power Sourcess*, 2009, **193**, 822-827.
221. M. M. Doeff, Y. Hu, F. McLarnon and R. Kostecki, *Electrochem. Solid-State Lett.*, 2003, **6**, A207-A209.
222. H. M. Xie, R. S. Wang, J. R. Ying, L. Y. Zhang, A. F. Jalbout, H. Y. Yu, G. L. Yang, X. M. Pan and Z. M. Su, **,** *Adv. Mater.*, 2006, **18**, 2609-2613.
223. Y. Hu, M. M. Doeff, R. Kostecki and R. Fiñones, *J. Electrochem. Soc.*, 2004, **151**, A1279-A1285.
224. R. Dominko, M. Belea, M. Gaberscek, M. Remskar, D. Hanzel, S. Pejovnik and J. Jamnika, *J. Electrochem. Soc.*, 2005, **152**, A607-A610.
225. V. Aravindan, K. Karthikeyan, J. W. Lee, S. Madhavi and Y. S. Lee, *J. Phys. D Appl. Phys.,* 2011, **44**, 152001-152004.
226. Z. Feng, J. Yang, Y. NuLi and J. Wang, *J. Power Sources*, 2008, **184**, 604-609.
227. S. Zhang, C. Deng and S. Yang, *Electrochem. Solid-State Lett.*, 2009, **12**, A136-A139.
228. L. Wenganga, X. Yunhuaa and Y. Rong, *Rare metals*, 2010, **29**, 511-514.
229. L. Qu, S. Fang, L. Yang and S.-i. Hirano, *J. Power Sources*, 2012, **217**, 243-247.
230. T. Kawase and H. Yoshitake, *Microporous Mesoporous Mater.*, 2012, **155**, 99-105.
231. K. Gao, J. Zhang and S.-D. Li, *Mater. Chem. Phys.*, 2013, **139**, 550-556.
232. X. Li, Y. Liu, Z. Xiao, W. Guo and R. Zhang, *Ceram. Int.*, 2014, **40**, 289-296.
233. R. Dominko, M. Bele, A. Kokalj, M. Gaberscek and J. Jamnik, *J. Power Sources*, 2007, **174**, 457-461.
234. L. Hong and Z. Zhang, *Russ. J. Electrochem.*, 2012, **49**, 386-390.
235. S. Zhang, C. Deng, F. L. Liu, Q. Wu, M. Zhang, F. L. Meng and H. Gao, *J. Electroanal. Chem.*, 2013, **689**, 88-95.
236. W. Chen, M. Lan, D. Zhu, C. Wang, S. Xue, C. Yang, Z Li, J. Zhang and L. Mi, *RSC Adv.*, 2013, **3**, 408-412.
237. X. Kong, T. Mei, Z. Xing, N. Li, Z. Yuan, Y. Zhu and Y. Qian, *Int. J. Electrochem. Sci.*, 2012, **7**, 5565-5573.
238. Y. Zhao, J. X. Li, N. Wang, C. X. Wu, Y. H. Ding and L. L. Guan, *J. Mater. Chem.*, 2012, **22**, 18797-18800.
239. Q. Zhang, X. Wang, W. Lu, F. Tang, J. Guo, W. Yu, L. Qu and Z. Yu, *Mater. Res. Bull.*, 2013, **48**, 2865-2870.
240. G. Wang, H. Li, Q. Zhang, Z. Yu and M. Qu, *J. Solid State Electrochem.*, 2010, **15**, 759-764.
241. Y. Zhao, J. Li, N. Wang, C. Wu, Y. Ding and L. Guan, *J. Mater. Chem.*, 2012, **22**, 18797-18800.
242. M. Molenda, M. Świętosławski, A. Wach, D. Majda, P. Kuśtrowski and R. Dziembaj, *Solid State Ionics*, 2014, **262**, 98-101.
243. X. Wu, X. Wang and Y. Zhang, *ACS Appl. Mater. Interface*, 2013, **5**, 2510-2516.
244. S. Devaraj, M. Kuezma, C. T. Ng and P. Balaya, *Electrochim. Acta*, 2013, **102**, 290-298.
245. Y. Lin, Y. Lin, T. Zhou, G. Zhao, Y. Huang and Z. Huang, *J. Power Sources*, 2013, **226**, 20-26.
246. K. Karthikeyan, V. Aravindan, S. B. Lee, I. C. Jang, H. H. Lim, G. J. Park, M. Yoshio and Y. S. Lee, *J. Power Sources*, 2010, **195**, 3761-3764.
247. X.-L. Wu, L.-Y. Jiang, F.-F. Cao, Y.-G. Guo and L.-J. Wan, *Adv. Mater.*, 2009, **21**, 2710-2714.
248. C. Sirisopanaporn, R. Dominko, C. Masquelier, A. R. Armstrong, G. Mali and P. G. Bruce, *J. Mater. Chem.*, 2011, **21**, 17823-17831.
249. Z. Chen, S. Qiu, Y. Cao, J. Qian, X. Ai, K. Xie, X. Hong and H. Yang, *J. Mater. Chem.,* 2013, **1**, 4988-4992.
250. M. K. Devaraju, T. Tomai, A. Unemoto and I. Honma, *RSC Adv.*, 2013, **3**, 608-615.
251. M. Wagemaker, B. L. Ellis, D. Lützenkirchen-Hecht, F. M. Mulder and L. F. Nazar, *Chem. Mater.*, 2008, **20**, 6313-6315.
252. S. Y. Chung, J. T. Bloking and Y. M. Chiang, *Nat. Mater.*, 2002, 123-128.
253. P. S. Herle, B. Ellis, N. Coombs and L. F. Nazar, *Nat. Mater.*, 2004, **3**, 147-152.
254. J. Hong, C. S. Wang, X. Chen, S. Upreti and M. Whittinghama, *Electrochem. Solid-State Lett.*, 2009, **12**, A33-A38.
255. S. Wang, K. Huang, B. Zheng, J. Zhang and S. Feng, *Mater. Lett.,* 2013, **101**, 86-89.
256. N. Meethong, Y.-H. Kao, S. A. Speakman and Y.-M. Chiang, *Adv. Funct. Mater.*, 2009, **19**, 1060-1070.
257. B. Xu, D. Qian, Z. Wang and Y. S. Meng, *Mater.Sci.Eng. B*, 2012, **73**, 51-65.

258. M. S. Islam, D. J. Driscoll, C. A. J. Fisher and P. R. Slater, *Chem. Mater.*, 2005, **17**, 5085-5092.
259. C. A. Fisher, V. M. Hart Prieto and M. S. Islam, *Chem. Mater.*, 2008, **20**, 5907-5915.
260. B. Ellis, P. Subramanya Herle, Y. H. Rho, L. F. Nazar, R. Dunlap, L. K. Perry and D. H. Ryan, *Faraday Discussions*, 2007, **134**, 119-141.
261. K. Zaghib, A. Mauger, J. B. Goodenough, F. Gendron and C. M. Julien, *Chem. Mater.*, 2007, 19, 3740-3747.
262. M. Wang, M. Yang, L. Ma and X. Shen, *RSC Adv.,* 2015, **5**, 1612-1618.
263. S. Choi, S. J. Kim, Y. J. Yun, S. S. Lee, S.-Y. Choi and H.-K. Jung, *Mater. Lett.,*2013, **105**, 113-116.
264. J. Thomas, T. Gustafsson, L. Häggström, A. Liivat, M. Dahbi, K. Kam and D. Ensling, *GCEP Technical Report* 2010.
265. M. Armand and M. Arroyo-de Dompablo, *J. Mater. Chem.,* 2011, **21**, 10026-10034.
266. M. Arroyo-de Dompablo, U. Amador and F. Garcia-Alvarado, *J. Electrochem. Soc.*, 2006, **153**, A673-A678.
267. D. H. Seo, Y. U. Park, S. W. Kim, I. Park, R. A. Shakoor and K. Kang, *Phys. Rev. B*, 2011, **83**, 205127.
268. A. Liivat and J. O. Thomas, *Comput. Mater. Sci.*, 2010 **50**, 191-197.

Table of contents graphic:

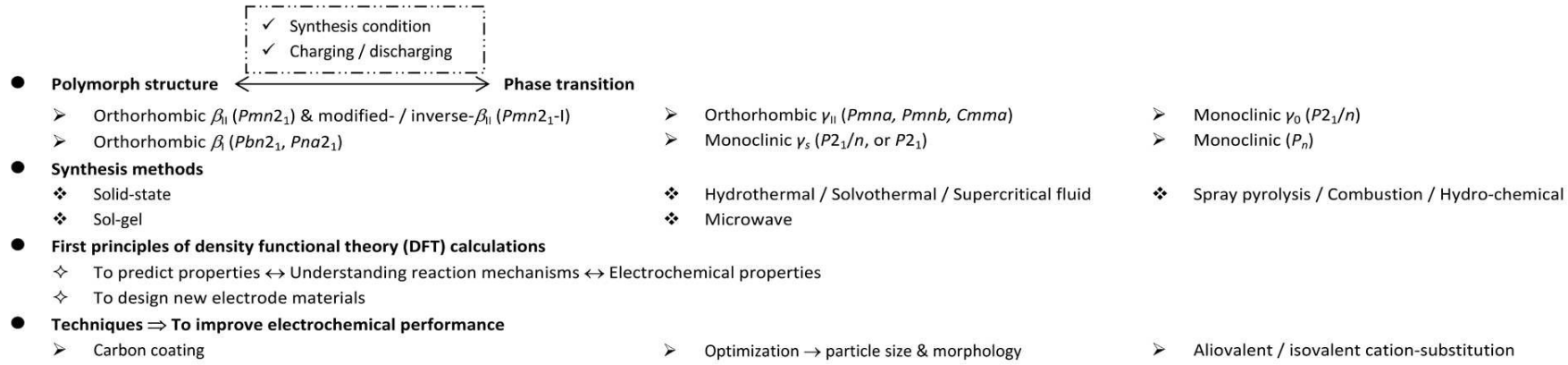

- This review highlights the high-capacity Li_2MSiO_4 (*M* = Mn, Fe, Co, Ni...) cathode material for lithium-ion batteries